ELECTROMAGNETIC TRANSIENT SOUNDINGS ON THE EAST RIFT GEOTHERMAL AREA OF KILAUEA VOLCANO, HAWAII: A STUDY OF INTERPRETATIONAL TECHNIQUES

A THESIS SUBMITTED TO THE GRADUATE DIVISION OF THE UNIVERSITY OF HAWAII IN PARTIAL FULFILLMENT OF THE REQUIREMENTS FOR THE DEGREE OF

MASTER OF SCIENCE

IN GEOLOGY AND GEOPHYSICS

DECEMBER, 1976

By

James Kauahikaua

Thesis Committee:

Gordon A. Macdonald, Chairman
George Sutton
Augustine Furumoto
Frank Peterson
Douglas Klein

ACKNOWLEDGEMENTS

The author wishes to thank Dr. Douglas Klein for his kind and thoughtful guidance over the last three years. He has been both patient and generous in sharing his thorough knowledge of the subject. I would also like to thank Drs. Robert Harvey and Mark Odegaard along with the members of my thesis committee listed on the title page. The investigation and thesis could not have been successfully completed without the help of the following people: Carroll Dodd for designing, building and testing the special electronic equipment required for transient sounding, Steve Thede, Darrel Kohara and Steve Minoha for assisting with the field work, Edwin Sakoda for doing the meticulous drafting and Mrs. Aileen Kauahikaua for painstakingly typing the final manuscript.

ABSTRACT

Seventeen electromagnetic transient soundings were done on the lower east flank of Kilauea volcano, Hawaii. Each sounding is based on the response of the earth as a function of time to a step function of current in a horizontal linear source. Interpretation of these response measurements is usually done by matching the data to standard model curves or asymptotic expressions; however, these methods presuppose that each datum has been measured with a relative precision (e.g. a precision of 5%) whereas, for transient sounding, each datum is commonly measured with an absolute precision (e.g. a precision of 10 μv). Therefore, a general inversion technique based on linear comparisons between the data and model values was used for the interpretations of the data in this study. The resulting geoelectric model shows that the structure is uniform vertically to a depth of 1000 m below sea level. There are broad, but distinct, lateral variations in the interpreted conductivity values ranging from 0.10 to 0.16 mho/m in most of east Puna to anomalous values of 0.30 to 0.50 mho/m in a particular area south of the rift at Puu Honuaula (see Figure 7). Based on these conductivity estimates, groundwater temperatures in the anomalous area are not expected to exceed 150° C to depths of 1000 m below sea level.

TABLE OF CONTENTS

	Page
ACKNOWLEDGEMENTS	iii
ABSTRACT	iv
LIST OF TABLES	vi
LIST OF FIGURES	vii
LIST OF SYMBOLS	ix
I. INTRODUCTION	1
II. EQUATIONS GOVERNING TRANSIENT SOUNDING	9
III. DATA ACQUISITION AND ANALYSIS	15
IV. INTERPRETATION AND RESULTS	22
Partial Inversion	27
Curve-Matching	38
Asymptotic Evaluation	39
Estimation by Half-Amplitude Decay Time	43
Evaluation and Comparison of the Interpretational Methods	44
V. GEOELECTRIC STRUCTURE AND GEOLOGICAL IMPLICATIONS	50
VI. CONCLUSIONS	59
APPENDIX A: FIELDS ABOUT A FINITE-LENGTH HORIZONTAL CURRENT SOURCE	60
APPENDIX B: TRANSIENT DATA PLOTS	67
APPENDIX C: COMPUTER PROGRAM LISTINGS	80
REFERENCES	86

LIST OF TABLES

		Page
Table I	Principal Facts and Statistics of Puna Transient Sounding Data	17
Table II	Summary of Transient Sounding Interpretations	53

LIST OF FIGURES

Page

Main Text

Figure 1 The major structural features and reported water temperatures in Puna 3

Figure 2 An idealized visualization of a transient sounding equipment setup and a typical set of source current and the corresponding sensor coil voltages 5

Figure 3 Source and sensor locations for transient soundings 23

Figure 4 The polarity and magnitude of the initial peak maximum of the two-layer perturbation response plotted versus its normalized arrival time 31

Figure 5 A plot of the data and best-fit halfspace model and the residuals for sounding 5 36

Figure 6 A plot of the early- and late-time asymptotic expressions and their interpretations for sounding 5 41

Figure 7 A map of the study area with the interpreted conductivities for each sounding plotted at the midpoint between source and sensor 57

Appendices

Figure A.1 Effects upon transient sounding interpretations for measurements taken close to the source . . . 63

Figure A.2 The transient response of the vertical magnetic field observed over a conductive halfspace close to a horizontal current source 65

Figure B.1 The transient sounding data plotted with the best-fit halfspace response as voltage versus time 68

Figure B.2 The data residuals plotted versus time 74

LIST OF FIGURES (CONT.)

Page

Figure B.3 The late-time resistivity functions for the transient data plotted in Figure B.1 78

LIST OF SYMBOLS

ℓ	:	length of the horizontal current source (m)
r	:	distance between current source and coil sensor (m), $r^2 = x^2 + y^2$
t	:	time (seconds)
σ	:	conductivity (mho/m)
σ_i	:	σ of the i^{th} layer, $\sigma_0 = 0$
d	:	thickness of the first layer of a two-layer earth (m)
d_i	:	thickness of the i^{th} layer
δ	:	skin depth (m), $\delta = \sqrt{2/\mu_0 \sigma \omega}$
μ	:	magnetic permeability (henry/m)
μ_i	:	μ of the i^{th} layer, $\mu_0 = 4\pi \times 10^{-7}$
ϵ	:	dielectric permittivity (farad/m)
ϵ_i	:	ϵ of the i^{th} layer, $\epsilon_0 = 8.852 \times 10^{-12}$
ω	=	$2\pi f$ (radians)
f	:	frequency (Hz)
$\vec{B}$	:	magnetic induction (teslas)
$\vec{E}$	:	electric field (volts/m)
$\vec{A}$	:	vector potential
U	:	scalar potential
k^2	=	$\omega^2 \mu \epsilon + i\omega\mu\sigma$
k_i^2	=	$\omega^2 \mu_i \epsilon_i + i\omega\mu_i\sigma_i$
J_1	:	Bessel function of the first kind of order one
N	:	number of layers in a multilayer earth model
R(m)	:	impedance function defined by equation II.7

$u = (r/2)\sqrt{\mu_o \sigma / t}$

$\mathrm{erf}(u) = (2/\sqrt{\pi}) \int_0^u e^{-x^2} dx$

$\mathcal{L}[\,]$: Fourier transform

n_t : number of turns enclosed by sensor coil

A : area enclosed by sensor coil (m^2)

$\overline{v}(t)$: transient voltage data (volts)

s^2 : data variance, see equation III.2

ν : number of degrees of freedom in s^2 estimate

n : number of data points in logarithmically resampled transient data set

$f(t,\vec{\theta})$: transient voltage model for the parameters $\vec{\theta}$

$\vec{\theta}$: model parameters

p : number of model parameters

$S(\vec{\theta})$: sum of squares of the residuals function defined by equation IV.3

$\theta_2 = 3Iyn_t A/2\pi\sigma_1 r^5$

$\theta_3 = r\sqrt{\mu_o \sigma_1}$

$\sigma_{\theta_2} = 3Iyn_t A/2\pi\ \hat{\theta}_2 r^5$

$\sigma_{\theta_3} = (\hat{\theta}_3/r)^2/\mu_o$

$\hat{\theta}_2, \hat{\theta}_3$: best-fit estimates of θ_2, θ_3

$\hat{\tau} = 2t/\mu_o \sigma_1 r^2$

$\mathrm{cor}(\vec{\theta})$: parameter correlation matrix

$\mathrm{cov}(\vec{\theta})$: parameter covariance matrix

$F(\vec{\theta})$: standard comparison of variances function

ρ : resistivity (ohm m), $\rho = 1/\sigma$

σ_ω : pore water conductivity (mho/m)

T : temperature (° C)

S : salinity (ppt)

I. INTRODUCTION

The main purpose of this investigation is to study the feasibility of using the electromagnetic transient sounding method to define the subsurface conductivity structure in a volcanic area. To this end, transient sounding data were obtained on the east flank of Kilauea volcano, Hawaii (Figure 1) in 1974 as part of a multidisciplinary geothermal exploration program conducted by the Hawaii Institute of Geophysics. The data was interpreted using several different techniques. The results provide a basis for evaluating the transient sounding method for geothermal exploration on Hawaii Island.

Transient sounding refers to measurements of the time-variations of electromagnetic fields which are generated by an electric source whose current is varied in a controlled manner with time. The source used here is a finite-length horizontal linear source whose current is varied in the form of a step function with time (see Figure 2). The magnetic field associated with such a source induces secondary electrical currents in the earth's conducting regions whose amplitude and rate of decay is controlled by the subsurface conductivity structure. Surface measurements of either the electric field or the associated magnetic fields, in conjunction with knowledge of the source fields, provide response data which can be used to determine the conductivity structure. In this study, time-variations of the vertical magnetic field were measured as voltages which were induced in a horizontal sensing coil. A typical setup along with idealized diagrams of the source current and the corresponding sensor voltage functions is

shown in Figure 2.

Inductive methods, such as transient sounding, should be able to accurately measure the high conductivities associated with geothermal resources while being relatively unaffected by the low overburden conductivities which can severely limit penetration by direct-current methods (Keller, 1970). Specifically, a transient survey should be able to detect a conductivity discontinuity at a depth between $\delta/16$ and δ (a skin depth), where

$$\delta = \sqrt{\frac{2}{\mu_0 \sigma \omega}}$$

σ is the conductivity above discontinuity

$\mu_0 = 4\pi \times 10^{-7}$ henry/m

$\omega = 2\pi f$

and f is frequency (Hz), with a resolution sufficient to determine both the conductivities above and below the discontinuity (Mundry, 1966). If the discontinuity is shallower than $\delta/16$ then the response will be that of a halfspace with the conductivity of the material below. If the discontinuity is deeper than δ, then the response will be that of a halfspace with the conductivity of the material above.

Transient sounding surveys on Kilauea volcano's summit (Jackson and Keller, 1972) and lower east rift zone (Skokan, 1974) and California's Long Valley (Stanley et al., 1976) have demonstrated that the method can be used to obtain large amounts of data for geothermal exploration purposes both quickly and economically. However, the Kilauea interpretations proved to be inadequate descriptions of subsurface conditions when compared with the results of deep research

Figure 1. The major structural features and reported water temperatures in Puna. The numbers above the well temperature symbols are the well reference numbers. The wells referenced by Roman numerals are geothermal test borings (Stearns, 1965).

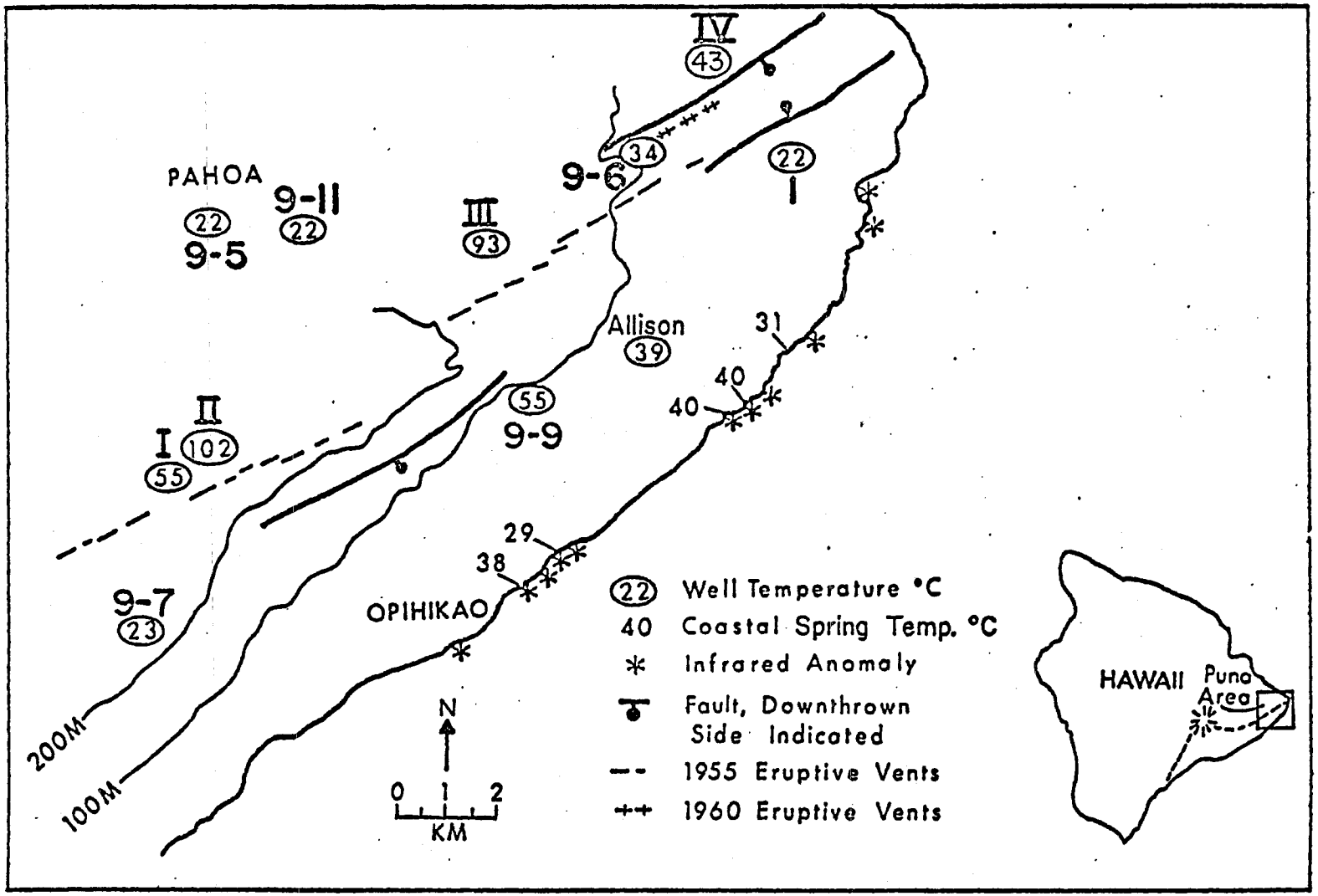
IV
43
34
9-6
22
PAHOA
9-11
22
22
9-5
III
93
Allison
39
31
40
40
55
9-9
II
I
102
55
29
38
9-7
23
OPIHIKAO
200M
100M
N
0 1 2
KM
22 Well Temperature °C
40 Coastal Spring Temp. °C
Infrared Anomaly
Fault, Downthrown Side Indicated
1955 Eruptive Vents
1960 Eruptive Vents
HAWAII
Puna Area

Figure 2. An idealized visualization of a transient sounding equipment setup showing a typical set of source current and sensor coil voltage functions. The setup is over a two-layer earth model.

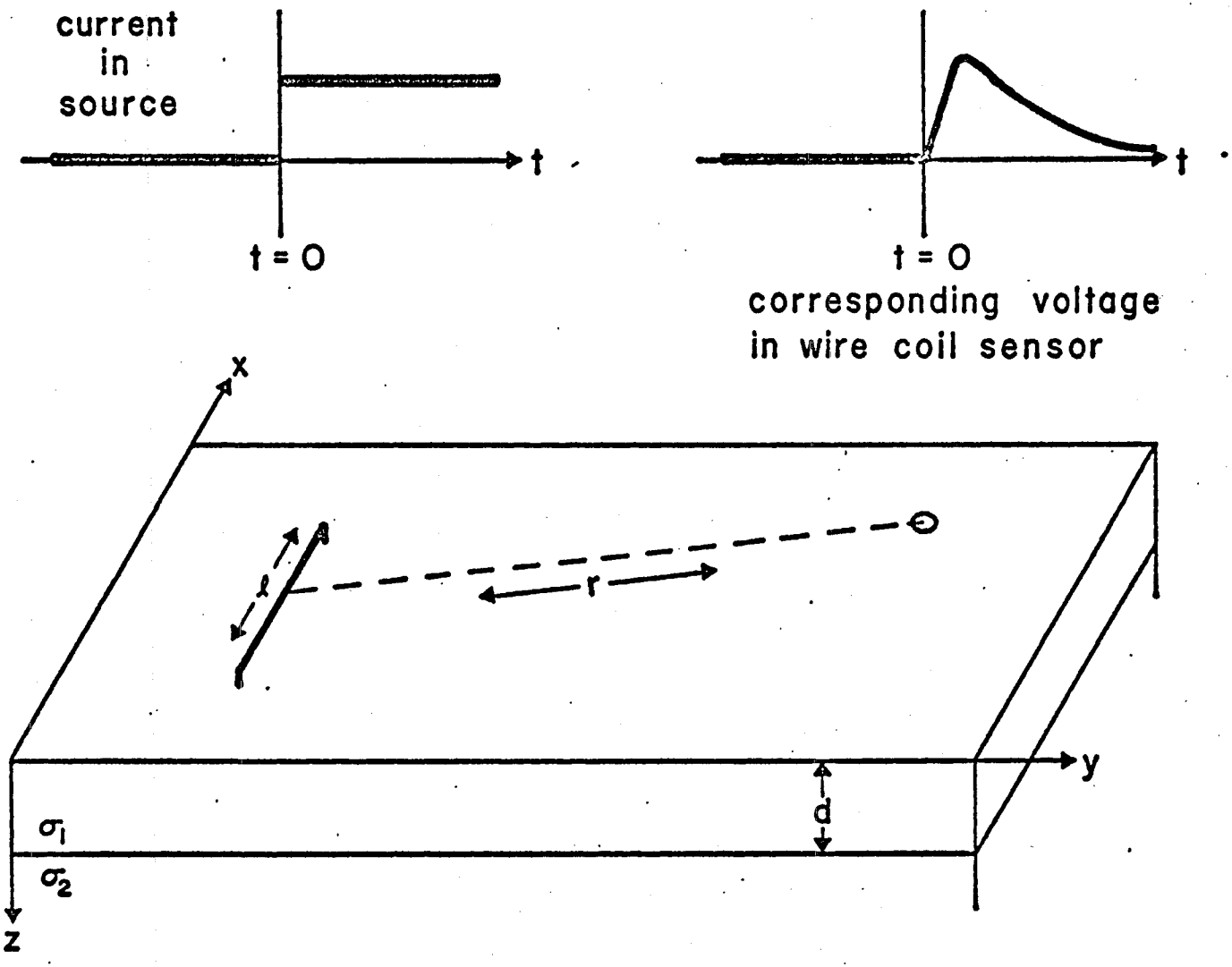
current
in
source
t
t = 0
t
t = 0
corresponding voltage
in wire coil sensor
x
A
l
r
y
d
σ_1
σ_2
z

drill holes in each area (Zablocki et al., 1974; G. A. Macdonald, personal communication, 1976). The reason for the failure of these interpretations may be that the interpretational techniques worked with the logarithms of the data values instead of the actual values. This procedure emphasizes small voltages and deemphasizes large ones, and may therefore suggest more complicated models than would ordinarily be necessary to fit the data. This possibility prompted the introduction and use of an interpretational approach, called partial inversion, which compares the actual data and model values by the least-squares criterion. Conventional interpretations, as well as interpretations which are based on asymptotic approximations to the theoretical model equations and half-amplitude decay times are also included to broaden the range of interpretational methods being evaluated.

Kilauea is an active, basaltic shield volcano situated on the southeastern portion of Hawaii Island and has two rift systems extending from the summit towards the southwest and east, respectively. The data to be interpreted in this study are from 17 transient soundings that were made on the lower east rift zone (east Puna District, see Figure 1). At the surface, the rift is a linear zone at least three kilometers wide and is marked by steam seeps, recent volcanic extrusions, cinder and spatter cones and pit craters. Below the surface, the rift is a dense complex of thin (less than 2 m), nearly vertical dikes (Macdonald, 1956) which may extend to depths of 2 to 5 km (Fiske and Kinoshita, 1969). The structure away from the rift is essentially horizontal and is the result of thick accumulations of

lava erupted from the rift.

Groundwater in Hawaii normally occurs in a Ghyben-Herzberg lens configuration with fresh water floating on salt water within the permeable mass of the island (Macdonald and Abbott, 1970). This lens certainly occurs in east Puna, but is apparently absent between the coast and the rift northeast of Opihikao (see Figure 1). The two wells in this area yield warm, brackish water with temperatures of 39° and 55° C and salinities in excess of 1000 ppm (McMurtry et al., 1976). Several warm basal springs have been discovered along the coast by infrared imagery (Fischer et al., 1966); some have been measured between 29° and 40° C. Along the rift trace, wells yield water with temperatures of 34° up to 102° C (Stearns, 1965). The groundwater lens appears to exist near Pahoa (wells 9-11 and 9-5) and southwest of Opihikao (well 9-7). Well 1, near the northeast tip of the area, appears to draw on water perched on ash.

Due to the general uniformity of Hawaiian lavas, electrical studies of the structure in Puna will respond primarily to the local groundwater conditions (Schwartz, 1937 and Zohdy and Jackson, 1969). The bulk conductivity of saturated lavas (and all other porous rock strata) is controlled by its porosity and the conductivity of its pore waters. The last is strongly affected by temperature, therefore detailed transient sounding studies of groundwater conditions may be able to provide details on thermal as well as structural abnormalities where groundwater is affected.

II. EQUATIONS GOVERNING TRANSIENT SOUNDING

An expression is sought here for the vertical magnetic field of a horizontal electric dipole on the surface of a horizontally layered earth. The theoretical development is initially in the frequency domain and the field has time dependence $e^{i\omega t}$. The final expression will be the transient, or temporal response to a step function of current through the electric dipole source. This development summarizes the detailed derivations of Vanyan (1967, p. 125) and Wait (1966 and 1951). SI (rationalized MKS) units are used within a cartesian coordinate system throughout.

Maxwell's equations in a homogeneous, charge-free medium are

$$\nabla \times \vec{B} = \mu\sigma\vec{E} + i\omega\mu\vec{E}\epsilon \qquad \text{(II.1)}$$

$$\nabla \times \vec{E} = -i\omega\vec{B} \qquad \text{(II.2)}$$

$$\nabla \cdot \vec{E} = 0 \qquad \text{(II.3)}$$

$$\nabla \cdot \vec{B} = 0 \qquad \text{(II.4)}$$

where $\vec{B}$ is the magnetic induction (teslas)

$\vec{E}$ is the electric field (volts/m)

$\omega = 2\pi f$

f is the frequency (Hz)

μ is the magnetic permeability (henry/m)

ϵ is the dielectric permittivity (farad/m)

and σ is the conductivity (mho/m) of the medium.

An explicit expression for $\vec{B}$ satisfying equation II.4 can be found by introducing the vector potential, $\vec{A}$, defined by

$$\vec{B} = \nabla \times \vec{A} \,. \qquad \text{(II.5A)}$$

Equation II.5A combined with equation II.2 yields

$$\vec{E} = -i\omega\vec{A} - \nabla U \qquad \text{(II.5B)}$$

where U is the electric scalar potential. Since $\vec{A}$ is defined somewhat arbitrarily by equation II.5A, we introduce the condition

$$U = -\frac{1}{i\omega\mu\epsilon}\nabla\cdot\vec{A}\,. \qquad \text{(II.5C)}$$

The vector potential satisfies the non-homogeneous wave equation,

$$\nabla^2\vec{A} - \mu\epsilon(i\omega)^2\vec{A} = -\mu\sigma\vec{E}$$

(as can be verified by combining equation II.1 with equations II.5A and II.5B) which may be rewritten using equation II.5C as

$$\nabla^2\vec{A} - k^2\vec{A} = -i\frac{\sigma}{\epsilon\omega}\nabla(\nabla\cdot\vec{A}) \qquad \text{(II.6)}$$

where $k^2 = \omega^2\mu\epsilon + i\omega\mu\sigma$. Equations II.5A through II.6 are completely equivalent restatements of Maxwell's equations, with the advantage that, for certain source configurations, we need only consider one or two components of $\vec{A}$ to specify all components of $\vec{E}$ and $\vec{B}$.

We assume that an electric dipole is situated at the origin of a cartesian coordinate system and oriented along the x-axis. The surface of an N-layered earth is at z=0 and the layer boundaries are planar and also perpendicular to the z-axis. The upper halfspace is assumed to be electromagnetically free space and its electrical properties are denoted by the subscript zero (e.g. $\epsilon = \epsilon_o$, $\mu = \mu_o$). The boundary conditions of continuity of the tangential components of $\vec{E}$ and the normal components of $\vec{B}$ and therefore the tangential

components of $\vec{A}$ and its derivatives can only be met if $\vec{A}$ has only non-zero x and z components (Wait, 1966). Solving these conditions, the vertical magnetic field is given by

$$B_z = \frac{I\mu_0}{2\pi}\left\{\frac{y}{k_1^2 r^5}\left[3-(3+3k_1 r+k_1^2 r^2)e^{-k_1 r}\right]+\frac{y}{r}\int_0^\infty m^2 R(m)J_1(mr)\,dm\right\} \quad (II.7)$$

where $\mu_0 = 4 \times 10^{-7}$ henry/m

$r^2 = x^2 + y^2$

$k_i^2 = -\omega^2\mu_i\epsilon_i + \omega\mu_i\sigma_i$

J_1 is a Bessel function of the first kind of order one

m is a variable of integration

$R(m) = R_{0,N}(m) - V_{0,1}$

$$R_{i-1,N}(m) = \frac{V_{(i-1),i} + R_{i,N}(m)\, e^{-2d_i V_i}}{1 + V_{(i-1),i} R_{i,N}(m) e^{-2d_i V_i}}$$

$R_{N,N}(m) = 0$

$V_{j,k} = (V_j - V_k)/(V_j + V_k)$

$V_j = m^2 + k_j^2$

ϵ_i is the dielectric permittivity of layer i

μ_i is the magnetic permeability of layer i

σ_i is the conductivity of layer i

and $k_0^2 \approx 0$ is assumed. We may further assume that σ_i will be always much larger than $\epsilon_i\omega$(the quasi-static assumption) and that $\mu_i = \mu_0$ for all layers; therefore, we may approximate k_i^2 as

$$k_i^2 \approx i\omega\mu_0\sigma_i \quad . \tag{II.8}$$

The first half in brackets of equation II.7 is the response of a halfspace of conductivity σ_1. The second half is the perturbation response due to layering.

For the setup in Figure 2, the vertical magnetic response of the earth to a step function of current in the source dipole is measured as a voltage induced in a wire coil. As an inductive sensor the coil responds to $\frac{\partial}{\partial t} b_z(t)$ rather than simply $b_z(t)$. The time function, $b_z(t)$, is related by the inverse Fourier transform to the frequency function of equation II.7, $B_z(\omega)$. The step function of current at the source is zero for negative times and a positive constant for times greater than or equal to zero. The source function is then $1/i\omega$, so

$$b_z(t) = \frac{1}{2\pi} \int_{-\infty}^{\infty} B_z(\omega) \frac{1}{i\omega} e^{i\omega t} d\omega = \mathcal{L}\left[\frac{B_z(\omega)}{i\omega}\right]$$

and

$$\frac{\partial}{\partial t} b_z(t) = \frac{1}{2\pi} \int_{-\infty}^{\infty} B_z(\omega) e^{i\omega t} \, d\omega = \mathcal{L}\left[B_z(\omega)\right] \quad . \tag{II.9}$$

Substituting equation II.7 into II.9 results in (Wait, 1951),

$$\frac{\partial}{\partial t} b_z(t) = \frac{I\mu_0}{2\pi} \left\{ \frac{3y}{\mu_0\sigma_1 r^5} \left[\mathrm{erf}(u) - \frac{2}{\sqrt{\pi}} \left(u + \frac{2}{3}u^3\right) e^{-u^2} \right] + \frac{y}{r} \cdot \right.$$
$$\left. \mathcal{L}\left[\int_0^{\infty} m^2 R(m) J_1(mr)\, dm \right] \right\} \tag{II.10}$$

where $u = \frac{r}{2}\sqrt{\frac{\mu_0\sigma_1}{t}}$ (t in seconds)

$$\mathrm{erf}(u) = \frac{2}{\sqrt{\pi}} \int_0^u e^{-x^2} dx \quad .$$

Again, the first half of equation II.10 is the halfspace response of conductivity σ_1 and is denoted below by $\frac{\partial}{\partial t} b_z^0(t)$. The second half is the perturbation of the transient response due to layering and is denoted by $\frac{\partial}{\partial t} b_z^P(t)$. Their separate expressions are

$$\frac{\partial}{\partial t} b_z^0(t) = \frac{3Iy}{2\pi\sigma_1 r^5}\left[\operatorname{erf}(u) - \frac{2}{\sqrt{\pi}}\left(u + \frac{2}{3}u^3\right)e^{-u^2}\right] \tag{II.11}$$

$$\frac{\partial}{\partial t} b_z^P(t) = \frac{I\mu_0 y}{2\pi r}\mathcal{L}\left[\int_0^\infty m^2 R(m)\, J_1(mr)\, dm\right] \tag{II.12}$$

$$\frac{\partial}{\partial t} b_z(t) = \frac{\partial}{\partial t} b_z^0(t) + \frac{\partial}{\partial t} b_z^P(t) .$$

Equation II.11 and II.12 have several properties worth noting at this stage in the development. For the halfspace response (II.11), if one starts at some finite, positive time,

$$\lim_{t\to 0} \frac{\partial}{\partial t} b_z^0(t) = \lim_{u\to\infty} \frac{\partial}{\partial t} b_z^0(t) = \frac{3Iy}{2\pi\sigma_1 r^5} \tag{II.13}$$

and

$$\lim_{t\to\infty} \frac{\partial}{\partial t} b_z^0(t) = \lim_{u\to 0} \frac{\partial}{\partial t} b_z^0(t) = 0 .$$

In words, the halfspace transient response goes instantaneously from zero to $3Iy/2\pi\sigma_1 r^5$ at zero time and subsequently decays back to zero with increasing time. For the perturbation response (equation II.12), if one again starts at some finite, positive time,

$$\lim_{t\to 0} \frac{\partial}{\partial t} b_z^P(t) = \lim_{\omega\to\infty} B_z^P(\omega) = 0 \tag{II.14}$$

$$\lim_{t\to\infty} \frac{\partial}{\partial t} b_z^P(t) = \lim_{\omega\to 0} B_z^P(\omega) = 0 \tag{II.15}$$

and

$$\lim_{t\to\infty} \int_0^t \frac{\partial}{\partial t} b^P(t)\, dt = \lim_{\omega\to 0} \frac{B_z^P(\omega)}{i\omega} = 0 \tag{II.16}$$

where $B_z^P(\omega) = \frac{I\mu_0 y}{2\pi r} \int_0^\infty m^2 R(m) J_1(mr)\,dm$.

The perturbation response is zero at time zero. For two or more layers, it departs from zero after time zero, but its integral with respect to time (the sum of the deviations from zero) and the perturbation response itself approaches zero as time increases. These properties will be important to the discussion of interpretation techniques which follows in chapter IV.

III. DATA ACQUISITION AND ANALYSIS

The transient sounding technique, as used here, is based on measurements of the time-variations of the vertical magnetic field of a horizontal current source. The current source is treated theoretically as an infinitesimal electric dipole, but it is physically realized as a single wire from 400 m to 1.4 km long which is grounded at each end with 20 to 40 steel stakes or electrodes (about 0.5 m long) connected in parallel and driven into the ground. Electrical ground contacts are sometimes improved by soaking the soil around the stakes with a mixture of salted water and highly-conductive drilling mud. Power is supplied by a three-phase 15 KVA diesel generator through a rectifier and automatic solid-state switcher connected in series with the wire and electrodes. During operation, the voltage is kept constant at nearly 1000 volts so the current is inversely proportional to the resistance measured between the electrodes. Due to the high resistivity of surface rocks in Puna, currents of only 2 to 6 amps are realizable although the equipment is capable of producing up to 15 amps. The switcher automatically turns the current on and off at a period of about 8.5 seconds, producing a continuous square wave signal. This period is longer than the time required for the transient response to decay to negligible voltage levels, so the step function idealization is valid.

Variations of the vertical magnetic field generated by this source are recorded as voltages induced in a square coil of wire laid horizontally on the ground. At the point of observation, the voltage

induced in the coil is related to the average magnetic field within the coil by

$$v(t)=n_t A \frac{\partial}{\partial t} b_z(t) \qquad \text{(III.1)}$$

where $v(t)$ is the transient voltage

n_t is the number of turns of wire in the coil

A is the area enclosed by the coil

and $b_z(t)$ is the transient vertical magnetic field. The coil used in this survey has 42 turns enclosing about 5800 m^2. To reduce natural ambient and cultural (60 Hz) noise, the transient voltages are recorded after passing through a one-pole low-pass filter (corner frequency of 4 Hz) and two band-reject filters (to reject 60 and 120 Hz) by a Hewlett-Packard oscillographic chart recorder capable of detecting one microvolt and recording at speeds up to 125 mm/sec.

From the chart records for each sounding, between 7 and 12 transients (defined as the voltage response to a single current step at the source) are manually digitized at 4 msec intervals for up to one second. Since each transient is actually a repeat measurement of the same response, they are stacked to obtain an average response, $\bar{v}(t)$. The stacking reduces noise and allows estimation of the data variance,

$$s^2 = \sum_{u=1}^{k} \sum_{i=1}^{n_u} [v_u(t_i) - \bar{v}(t_i)]^2 \qquad \text{(III.2)}$$

where k is the number of transients being stacked,

n_u is the number of voltage observations for transient u,

Table I. Principal Facts and Statistics of Puna Transient Sounding Data

Sounding	Source	r(m)	r/ℓ	$\cos^{-1}(y/r)$	$s^2(x10^{-8})$	ν	n
1	1	1678	2.4	75	84.40	1301	17
3	1	2620	3.8	66	1.36	1203	19
5	1	2750	4.0	71	33.90	1318	20
6	1	3140	4.6	65	2.05	1272	21
7	1	2500	3.6	60	9.27	906	15
14	2	2040	3.3	64	2.16	794	20
15	2	3500	5.6	54	.45	1899	21
16	2	3100	5.0	82	1.89	2350	19
23	3	1290	2.3	78	15.00	1188	19
24	3	2450	4.3	90	5.37	2591	25
25	4	1780	1.8	72	8.90	879	18
26	4	2080	2.1	80	10.60	990	20
27	4	3290	3.3	82	8.00	1589	17
28	4	2650	2.7	72	10.70	1224	19
29	4	3190	3.2	62	19.70	1101	16
30	4	4460	4.5	80	.69	2098	24
31	4	3700	3.7	63	1.07	1702	23

Definition of the parameters. The equations refer to the main text.

r : source to sensor distance in meters.

ℓ : source length in meters.

$\cos^{-1}(y/r)$: angle between the source direction and the line between source and sensor.

s^2 : data variance, equation III.2.

ν : degrees of freedom in s^2.

n : number of data points in the logarithmically resampled transient data set.

$v_u(t_i)$ is the voltage at time t_i, (i=1, 2,... n_u) for transient u

$\bar{v}(t_i)$ is the average voltage at time t_i,

and $\nu = \sum_{u=1}^{k} (n_u - 1)$ is the number of degrees of freedom for s^2

(Draper and Smith, 1966). The data standard deviation, s, is a statistical expression of the noise in the signal. The noise ratio, which is the largest observed voltage divided by s, can be used to compare the relative magnitude of noise in one signal to that in another signal. For our data, the noise ratios ranged from 4.2 to 74.6 and averaged about 12.

The averaged transient is not the true earth response, but rather the earth response distorted by the measuring and recording equipment. The distortion must be determined and the transient compensated before further analysis. The compensation is most easily dealt with as a division operation in the frequency domain rather than the equivalent convolution in the time-domain. The amount of distortion was estimated in the laboratory as the impulse response of the filters and the chart recorder, denoted $I(\omega)$. After stacking, each transient is transformed to the frequency domain, compensated using the relation

$$E(\omega) = \frac{V(\omega)}{I(\omega)}$$

where $E(\omega)$ is the earth response and $V(\omega)$ is the Fourier transform of $\bar{v}(t)$, and transformed again to the time-domain.

The result of the stacking and compensation procedures described above should be the true earth response. The resultant transients, however, are noisier than when originally measured. This can be

explained by aliasing of the original transient. The frequency range resolvable for a transient sampled at 4 msec intervals is 0 to 125 Hz. The filters used in recording produce only 37 db attenuation at 125 Hz while the dynamic range of the recorder is nearly 60 db. The transients as recorded on chart records can then contain significant amounts of signal at frequencies higher than the digital Nyquist limit of 125 Hz which are added to the transient and which affected the frequencies between 35 and 125 Hz (the range is empirically determined) by digitization (Jenkins and Watts, 1968). This problem was not discovered until after the data had been collected, and since accurate numerical compensation was not possible over the affected frequency range, the only remedy was to delete the aliased data. The compensation algorithm was amended so that, after compensation in the frequency domain, all components for frequencies higher than 35 Hz are set to zero before transformation back to the time domain. This procedure is equivalent to low-pass boxcar filtering in the frequency domain.

Conventional transient analysis requires that the earth response, now sampled at 4 msec intervals (e.g., at 4, 8, 12, 16, 20, 24 msec), be resampled at geometric intervals (e.g., at 4, 8, 16, 32, 64 msec). The shape of the response is not changed, but its digital form is shortened from between 125 and 250 points, to between 20 and 30 points, and is thus much more economical to work with on a computer. First, the portion of each transient in which initial build-up occurs (usually no more than the first 20 msec) is discarded leaving only the transient's long decay. The build-up must be removed as it is the

result of using only part of the frequency response and is not part of the earth response. Second, the long decay is averaged arithmetically over a band two intervals wide extending from the time

$$(4 \text{ msec}) \times 10^{.07(i-1)} \quad , \; i=10, 11, 12, \ldots$$

to the time $(4 \text{ msec}) \times 10^{.07(i+1)}$, $i=10, 11, 12, \ldots$

resulting in a shortened digital transient resampled at the times

$$(4 \text{ msec}) \times 10^{.07i} \quad , \; i=10, 11, 12, \ldots$$

The logarithmic interval of 0.07 is used so that none of the sampled intervals is ever shorter than 4 msec between 20 msec and 1 sec.

Jackson and Keller (1972) use a filter similar to this one to transform their arithmetically sampled transients to geometrically sampled ones, with the important exception that the transient is averaged logarithmically,

$$\bar{a} = \left(\prod_{i=1}^{m} a_i\right)^{1/m}$$

rather than arithmetically,

$$\bar{a} = \frac{1}{m} \sum_{i=1}^{m} a_i$$

as is done here. Their use of the logarithmic average appears superficially justified because the logarithmic average is equivalent to averaging the transient as it appears on a bilogarithmic plot. On closer examination, however, particular properties of the logarithmic average can render its estimates very inaccurate. The most obvious difficulty is with negative numbers which commonly occur in noisy

data. In this case, the roots of the logarithmic average expression above may not be real values. The final average may have no meaning with respect to the numbers it represents.

IV. INTERPRETATIONS AND RESULTS

Several interpretation methods have been used for transient sounding data. Many of these techniques as well as two new ones were utilized for the 17 soundings in Puna (located in Figure 3) so that comparisons could be made between the results. The conventional techniques discussed here are logarithmic curve-matching (in the time-domain) and early-time and late-time asymptote evaluation. The two new ones to be discussed are partial inversion, which can be used to determine the best-fit halfspace response, and a half-amplitude decay time method, which can be used in the field for quick determinations of apparent conductivity.

Both the logarithmic curve-matching and partial inversion methods use the sounding data to determine subsurface layering by minimizing the differences between the data and models. The difference between the two approaches is in their respective minimization criteria. With curve-matching, one minimizes the differences between the logarithm of the data value and the logarithm of the model value, e.g., minimizes the square of the residuals

$$\sum_{i=1}^{n} \left[\log \bar{v}(t_i) - \log f(t_i,\vec{\theta})\right]^2$$

$$= \sum_{i=1}^{n} \left[\log \frac{\bar{v}(t_i)}{f(t_i,\vec{\theta})}\right]^2 \qquad \text{(IV.1)}$$

where $\bar{v}(t_i)$ is the transient voltage data

$f(t_i,\vec{\theta})$ is the transient voltage model for the parameters in

Figure 3. Current source and sensor coil locations for the seventeen soundings in Puna.

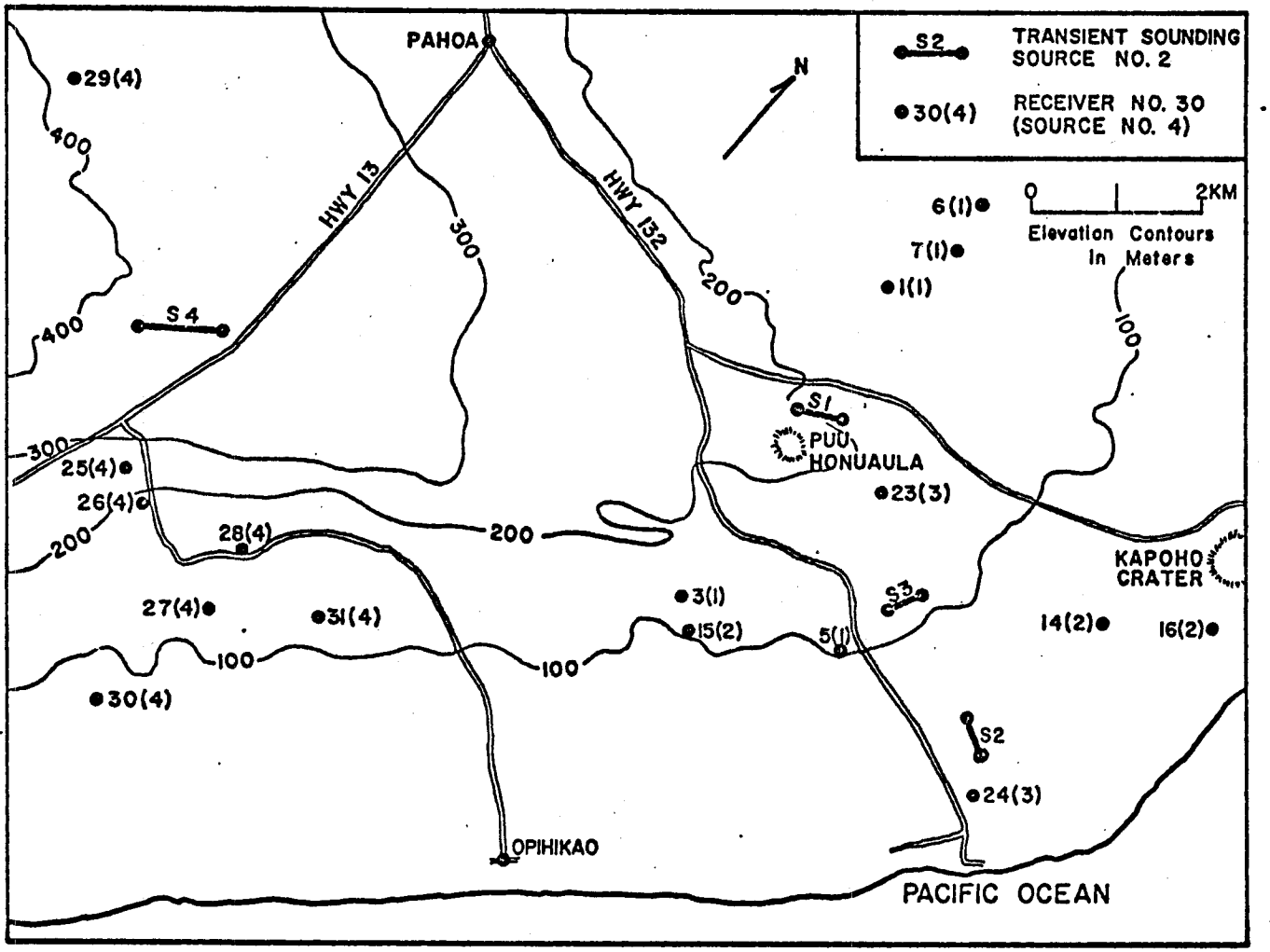
PAHOA
N
S2
TRANSIENT SOUNDING SOURCE NO. 2
30(4)
RECEIVER NO. 30 (SOURCE NO. 4)
0
2KM
Elevation Contours In Meters
HWY 13
HWY 132
29(4)
400
400
300
200
100
S4
S1
PUU HONUAULA
6(1)
7(1)
1(1)
23(3)
300
25(4)
26(4)
200
200
28(4)
KAPOHO CRATER
S3
3(1)
27(4)
31(4)
15(2)
5(1)
14(2)
16(2)
100
100
30(4)
S2
24(3)
OPIHIKAO
PACIFIC OCEAN

the vector $\vec{\theta}$

and t_i, i=1, 2,...n are the times at which data were measured. With the partial inversion method, one minimizes the squares of the differences between the actual data and model values, e.g. minimizes the squares of the residuals

$$\sum_{i=1}^{n} \frac{1}{(s_i)^2} \left[\overline{v}(t_i) - f(t_i,\vec{\theta})\right]^2 \qquad \text{(IV.2)}$$

where s_i^2 is the variance of $\overline{v}(t_i)$. Although equation IV.1 is a common minimization criterion for resistivity data, equation IV.2 is the general least-squares minimization criterion (Draper and Smith, 1966). Equation IV.1 is actually similar to a special case of equation IV.2 where the data standard deviation, s_i, is always proportional to $\overline{v}(t_i)$. This special case is commonly encountered in resistivity work where all data are measured with a relative precision of perhaps 5 percent. For this example, equation IV.2 yields

$$\frac{1}{(0.05)^2} \sum_{i=1}^{n} \left[1 - \frac{f(t_i,\vec{\theta})}{\overline{v}(t_i)}\right]^2$$

The above expression and equation IV.1 are both minimized by having the ratios of data and model values approach unity, rather than having their differences approach zero as in equation IV.2. Transient sounding data are measured with an absolute precision of perhaps 5 microvolts and should use equation IV.2 as it does not fit into the special case outlined above.

The overall approach of logarithmic curve-matching and partial inversion as used here differs from that of curve-matching methods in

most resistivity interpretation studies in that only the shape of the transient data curves are matched to the model curves. The amplitudes of transient data can be also used to determine the surface layer resistivity; however, studies of the effects of various kinds of errors on resistivity determination from transient data (Vanyan, 1967, p. 201) show that these errors affect transient amplitudes and shapes differently. For example, transient sounding theory, as outlined in chapter II, is developed for an infinitesimal, horizontal current source and wire coil receiver and applies to practical cases for which the maximum dimension of either source or receiver is less than one-fifth the distance between them (Keller and Frischknecht, 1966, p. 288). The halfspace model studies in Appendix A show that when the separation-length conditions are not fulfilled, such transients will still have the same basic form as predicted by the infinitesimal current source theory but they will not have the same amplitudes. Separate resistivity determinations of these transient models by amplitude and shape will differ from each other and from the real resistivity (see Figure A.1). In this case, if resistivity determination from shape and amplitude were constrained to yield the same surface layer resistivity, as Skokan (1974) has suggested, then the data might be interpreted to suggest two layers when in reality, the data is the response of a halfspace. Errors in the measurement of source length, current, receiver coil area or orientation can also have large effects upon the amplitude of a transient, but relatively small effects upon its shape. Resistivity determination will therefore be made independently by amplitude and shape and the resulting

estimates will be evaluated on their separate merits.

Partial Inversion

The ultimate interpretation technique for determining layer conductivities and thicknesses from transient sounding data is non-linear regression or inversion. In the few studies of inversion methods with electrical (other than transient) data, the technique was able to determine not only the layer parameters, but also their variances and covariances (e. g. Glenn et al., 1973 and Inman, 1975). For full transient data inversion, one seeks the set of parameters (layer conductivities and thicknesses) for which the sum-of-squares function

$$S(\vec{\theta}) = \sum_{i=1}^{n} \frac{1}{(s_i)^2}\left[\overline{v}(t_i) - f(t_i,\vec{\theta})\right]^2 \qquad \text{(IV.3)}$$

where $\overline{v}(t_i)$ is the digital transient voltage data

n is the number of transient data points

$f(t_i,\vec{\theta})$ is the transient voltage model

$= n_t A\left\{\frac{\partial}{\partial t} b_z^0(t_i) + \frac{\partial}{\partial t} b_z^P(t_i)\right\}$ (see equations II.11, II.12 and III.1),

is a minimum. The best-fit parameters (denoted $\hat{\vec{\theta}}$) can be specifically defined as the set of parameters for which

$$\left.\frac{\partial S(\vec{\theta})}{\partial \vec{\theta}}\right|_{\vec{\theta}=\hat{\vec{\theta}}} = 0.$$

Many algorithms have been developed for automatically minimizing equations like IV.3 but they all require iterative evaluations of the

model function, $f(t_i,\vec{\theta})$, and its derivatives with respect to the parameters for each inversion. Full inversion would then be prohibitively costly for transient data because each model and derivative evaluation would require the numerical computation of a double integral. A method of partial inversion was devised to separate the halfspace and perturbation components of the data for separate analysis (Yost, 1952). This method is as adequate as full inversion for two-layer interpretations (except that variances cannot be estimated statistically for perturbation interpretations) and is far cheaper than full inversion.

First, the transient data are inverted to determine the best-fit halfspace response with the following model (see equation II.11) of the parameters $(\theta_1,\theta_2,\theta_3)$:

$$f(t_i,\vec{\theta}) = \theta_1 + \theta_2\left[\operatorname{erf}(u) - \frac{2}{\sqrt{\pi}}(u + \frac{2}{3}u^3)e^{-u^2}\right] \qquad \text{(IV.4)}$$

where $u = \theta_3/2\sqrt{t_i}$

$$\theta_2 = \frac{3Iy}{2\pi\sigma_1 r^5} n_t A$$

$$\theta_3 = r\sqrt{\mu_o\sigma_1}.$$

The derivatives are

$$\frac{\partial}{\partial\vec{\theta}} S(\vec{\theta}) = -2 \sum_{i=1}^{n} \frac{1}{(s_i)^2}\left[v(t_i) - f(t_i,\vec{\theta})\right]\frac{\partial}{\partial\vec{\theta}} f(t_i,\vec{\theta}) \qquad \text{(IV.5)}$$

where $\frac{\partial}{\partial\theta_1} f(t_i,\vec{\theta}) = 1$

$$\frac{\partial}{\partial\theta_2} f(t_i,\vec{\theta}) = \operatorname{erf}(u) - \frac{2}{\sqrt{\pi}}(u + \frac{2}{3}u^3)e^{-u^2}$$

$$\frac{\partial}{\partial\theta_3} f(t_i,\vec{\theta}) = \theta_2\frac{4}{3\sqrt{\pi t_i}}e^{-u^2}u^4.$$

The first parameter, θ_1, is included in equation IV.4 so that the

base voltage (the ambient voltage upon which the transient voltage is superimposed) can be estimated as a parameter and need not be observed as a datum, and so that

$$\sum_{i=1}^{n} \frac{1}{(s_i)^2}\left[\bar{v}(t_i) - f(t_i,\vec{\theta})\right] = 0 = \frac{\partial}{\partial\theta_1} S(\vec{\theta})\Big|_{\vec{\theta}=\hat{\vec{\theta}}} .$$

This last property along with the observation that

$$\int_0^{\infty} \frac{\partial}{\partial t} b_z^P(t)dt = 0 \qquad \text{(equation II.16)},$$

are sufficient reasons to believe that the inversion can estimate and that the resultant residuals, defined by

$$r(t_i) = \bar{v}(t_i) - f(t_i,\vec{\theta}) \qquad \text{(IV.6)}$$

will contain the perturbation due to any deeper layers along with noise. The residuals can be used to estimate these deeper layer parameters. The transient, of course, must be sampled over a time span sufficient to include the beginning and end of the perturbation.

Davidon's method (Fletcher and Powell, 1963) was chosen as the inversion algorithm because it has quick and stable convergence properties and it estimates the second derivatives of $S(\vec{\theta})$ at $\hat{\vec{\theta}}$ for the proper computation of non-linear parameter covariances (Beale, 1960). Before inversion, the data were scaled so that θ_1, θ_2 and θ_3 would all be of equivalent magnitude as suggested by Bard (1963) for improved convergence.

Several two-layer model perturbation responses were calculated using a modified computer program published by Skokan (1974) in an

attempt to characterize them. The model responses were similarly shaped and showed an initial peak maximum followed by a smaller peak of opposite polarity (a sample response is plotted in Figure 4). For a constant surface layer thickness, the polarity of the initial peak indicates whether the ratio σ_2/σ_1 is greater than or less than unity (positive for σ_2/σ_1 1), while the peak amplitude increases with increasing departure of σ_2/σ_1 from unity. For a constant σ_2/σ_1, the peak amplitude decreases approximately exponentially and its arrival time increases linearly with increasing surface layer thickness. Since surface layer thickness and σ_2/σ_1 are uniquely defined by the polarity, amplitude and arrival time of the initial peak alone, this information was plotted in Figure 4 in lieu of the full model responses.

Partial inversion then consists of the following steps:

1. determine the best-fit halfspace response by minimizing equation IV.3 with the model in equation IV.4 using Davidon's method,

2. calculate two estimates of σ_1 (based on definitions of amplitude dependent θ_2 and shape dependent θ_3 in equation IV.4) by

$$\sigma_{\theta_2} = \frac{3Iyn_t A}{2\pi r^5 \hat{\theta}_2}$$
$$\sigma_{\theta_3} = (\hat{\theta}_3/r)^2/\mu_o \qquad \text{(IV.7)}$$

and calculate the residuals by equation IV.6,

3. test whether the residuals contain anything more than random noise by a runs test and a comparison of the residual amplitudes with the data standard deviation, s,

Figure 4. The polarity and magnitude of the first peak maximum of two-layer perturbation responses (as in equation II.12) plotted versus arrival time. The sample perturbation response is for the case of $k = \sigma_2/\sigma_1 = 4$ and $d/r = 0.375$. The abscissa is scaled to normalized time, $\tau = 2t/\mu_o \sigma_1 r^2$. For comparison with noise amplitudes, the ordinate would be equivalent to the reciprocal of the noise ratio.

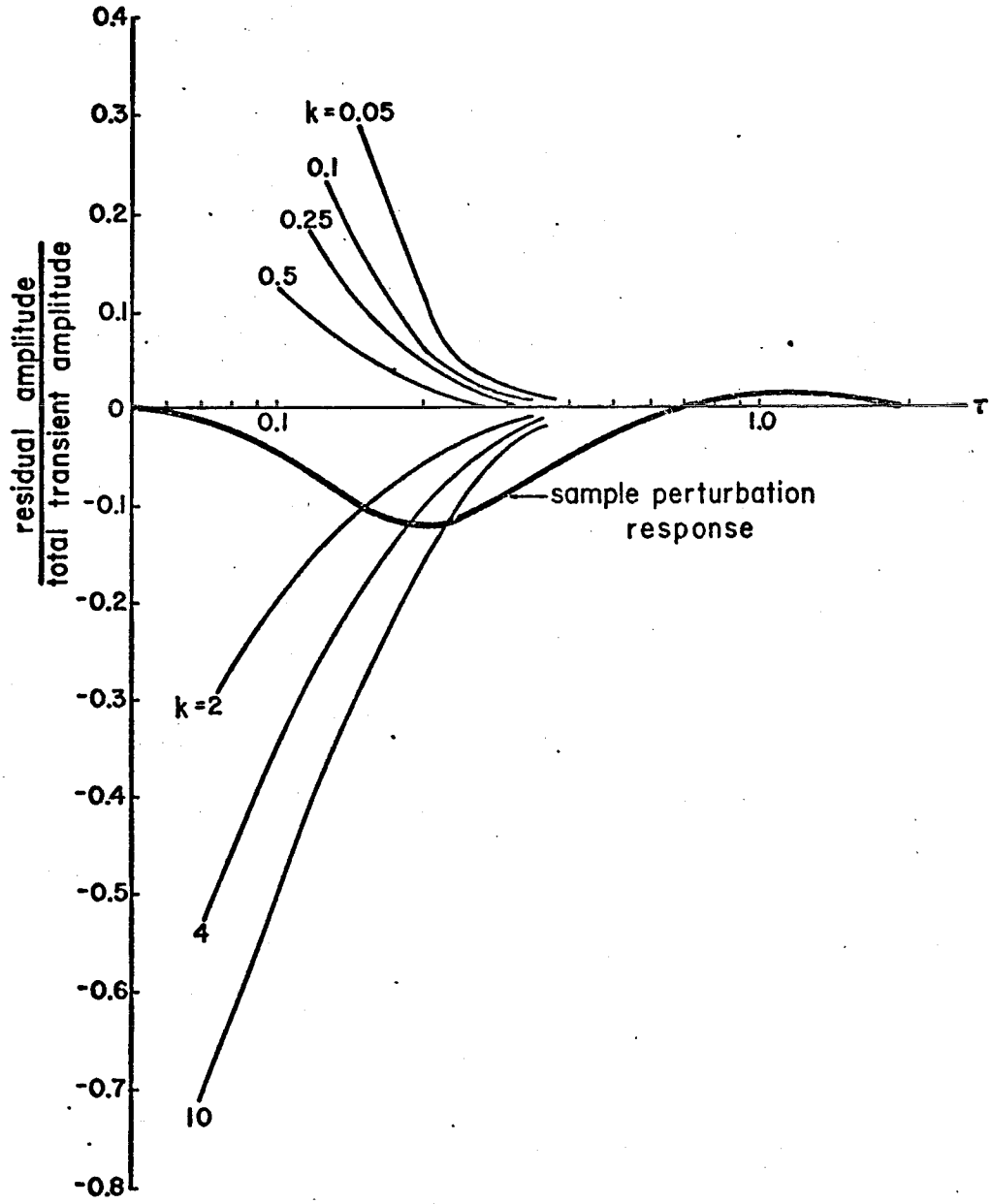
0.4
0.3
0.2
0.1
0
-0.1
-0.2
-0.3
-0.4
-0.5
-0.6
-0.7
-0.8
residual amplitude / total transient amplitude
k=0.05
0.1
0.25
0.5
0.1
1.0
τ
sample perturbation response
k=2
4
10

4. if the residuals seem to be more than noise and a perturbation model response shape is discernible, pick the time which corresponds to the initial peak maximum, t, and normalize it by

$$\tau = \frac{2t}{\mu_0 \sigma_1 r^2} \quad .$$

The surface layer thickness has been empirically determined to be $2r\tau$. Finally, divide the peak maximum's amplitude by $\hat{\theta}_2$ and plot it versus τ on Figure 4 to estimate σ_2/σ_1 .

The seventeen sets of logarithmically resampled transient voltage data were interpreted by partial inversion. Each resampled data point was weighted by the number of original data points which were used for its estimation in the resampling procedure (e. g. if the fifth resampled data point is the average of four of the original data points, then its weight in equation IV.3 is $4/s_5^2$ instead of $1/s_5^2$). When weighted in this way, resampled (and therefore smaller sets of) data are essentially the same as the original data and produce best-fit parameters within one percent of those produced by the original data. Iteration was stopped when each of the derivatives became less than 10^{-6} (usually within ten iterations) and the two estimates of σ_1 were calculated and are listed in Table II under "σ_{θ_2}" and "σ_{θ_3}". Standard deviations for each of the parameters were calculated as the square-root of the covariance, $\text{cov}(\hat{\bar{\theta}})$, given by

$$\text{cov}(\hat{\bar{\theta}}) = 2S^{-1} \qquad \text{(IV.8)}$$

where S^{-1} is the inverse of a 3 x 3 matrix whose elements are

$S_{ij} = \frac{\partial^2 S(\theta)}{\partial\theta_i \partial\theta_j}$, i,j = 1, 2, 3 (Beale, 1960), and which is provided by Davidon's minimization algorithm. The standard deviations are listed beside σ_{θ_2} and σ_{θ_3} in Table II. Each of the shortened transient data sets are plotted in Figure B.1 along with the best-fit halfspace model and the parameter correlation coefficients given by

$$[\mathrm{cor}(\hat{\theta})]_{ij} = \frac{[\mathrm{cov}(\hat{\theta})]_{ij}}{[\mathrm{cov}(\hat{\theta})]_{ii}^{1/2}[\mathrm{cov}(\hat{\theta})]_{jj}^{1/2}} \qquad \text{(IV.9)}$$

(Draper and Smith, 1966). A sample plot is presented in Figure 5 for sounding 5.

The agreement (within one standard deviation of σ_{θ_2}) between σ_{θ_2} and σ_{θ_3} for soundings 1, 3, 5, 6, 7, 16, 23, 24, 29, 30 and 31 (see Table II) suggests that a transient halfspace response model fits the basic trends in the data well for these soundings. The fit may be tested more quantitatively by a comparison of the sum-of-squares function minimum value, $S(\hat{\theta})$, and the data variance, s^2, for each sounding. A comparison of variances, commonly called an F-test, at the $(1-\alpha)$ confidence level is done by calculating $F(\hat{\theta})$ for each fit by

$$F(\hat{\theta}) = \frac{[(S(\hat{\theta}) - s^2)/(n - p - \nu)]}{s^2/\nu}$$

where n is the number of data points used in the fit

p=3 is the number of parameters used in the model

and ν is the number of degrees of freedom in the data variance estimate, and comparing it to the corresponding value in an F-table, denoted by $F_\alpha(n-p-\nu;\nu)$ (Draper and Smith, 1966, p. 306). The model

appears to explain the non-random elements of the data if $F(\hat{\theta})$ is less than or equal to $F_{\alpha}(n-p-\nu;\nu)$. For the eleven soundings listed above, $F(\hat{\theta})$ never exceeds 1.14 and the fit of the halfspace model appears to be adequate at the 95% confidence level.

For soundings 14, 26, 27 and 28, $F(\hat{\theta})$ is also less than 1.14, however, σ_{θ_2} is significantly less than σ_{θ_3}. The consistency of values for soundings 26, 27, 28, 30 and 31 (between 0.10 and 0.16 mho/m), which are located in the same area, and the goodness of fit of the halfspace model suggests that the discrepancy between σ_{θ_2} and σ_{θ_3} for soundings 26, 27 and 28 is probably the result of the measurement error effects discussed earlier. σ_{θ_3} is assumed to be the best estimate of σ_1 in this case. The $F(\hat{\theta})$ value exceeds 1.14 for the last two soundings (15 and 25) and indicates that the halfspace model fit is inadequate. Since σ_{θ_2} differs from σ_{θ_3} by a factor of at least two for soundings 15 and 25 also, we may conclude that these two soundings will not benefit from partial inversion interpretation.

The test for randomness were done on the residuals at the 95% confidence level. Soundings 15, 16, 24, 26, 27, 30 and 31 contain too few runs (common sign groups in the sequence) to accept randomness. Soundings 3, 6, 16, 25, 26, 27, 28, 30 and 31 contain residual values in excess of 1.96s, the 95% confidence level limit. The largest residual values were always the earliest two or three points, which is typical of distortions due to coil misorientation or to thin, low conductivity surface layers (Vanyan, 1967, p. 201), but not of perturbations due to layering. Because of the generally small amplitude of

Figure 5. A plot of the data and best-fit halfspace model and the residuals for sounding 5. The ordinate for the residual plot is the voltage divided by $\hat{\theta}_2$.

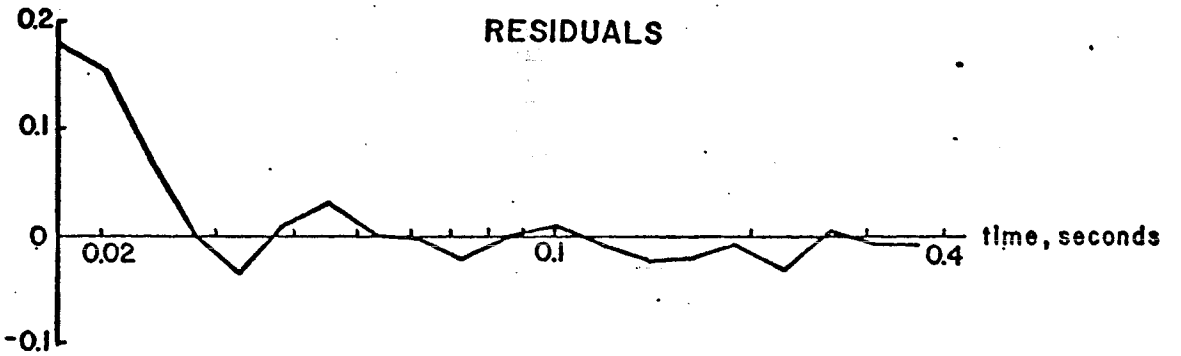

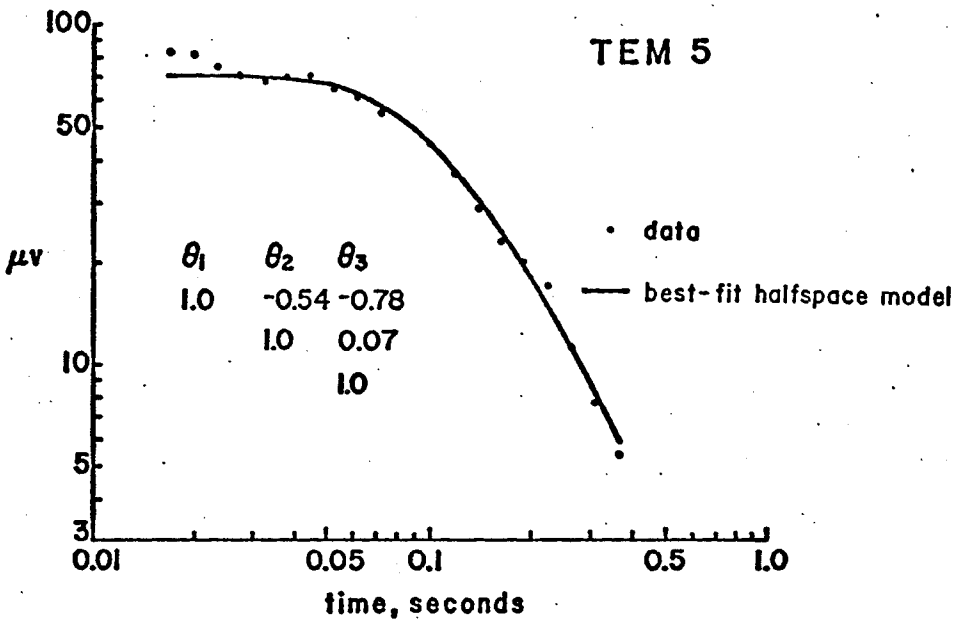

the residuals and the lack of resemblance to perturbation model shapes, the residuals were not analyzed further. A sample residual is plotted in Figure 5 for sounding 5. Residuals for all the soundings are plotted in Figure B.2.

Figure 4 has another use besides interpretation with partial inversion. It can be used to quantitatively determine the limits of resolution of the transient sounding method. For example, with data having a noise ratio of 10 to 15 (like most of the Puna data in this study), it would be very difficult to distinguish a perturbation response from noise if σ_2/σ_1 is between 0.05 and 10 and the surface layer thickness is greater than half the source-sensor separation, r. This would appear to raise grave doubts about the possible detection of small conductivity discontinuities (σ_2/σ_1 of about 0.2 to 0.5) at depths of 2 km or more as reported in Puna by Skokan (1974).

The results of partial inversion show that 15 of the 17 transient data sets can be most simply and adequately interpreted as halfspace responses. There is no question that an interpretation with more layers, as Skokan (1974) suggests, would be possible; however, the quality of the data could not support the added model complexity.

Curve-Matching

The transient data are first converted from voltages to apparent resistivities by

$$\rho_a = \frac{2\pi r^5}{3Iyn_t A}\,\bar{v}(t) \qquad \text{(IV.10)}$$

and plotted bilogarithmically versus time. The data curves are then

Matched to model curves which are standardly plotted as ρ_a/ρ_1 versus normalized time, τ, given by

$$\tau = \frac{2\rho_1}{\mu_o r^2} t$$

where $\rho_1 = 1/\sigma_1$ and t is the time in seconds. Two-layer model sets have been published by Silva (1969), three-layer model sets by Skokan (1974) and four-layer model sets by Vanyan (1967). Computer programs for the numerical calculation of multi-layered models have been published by Skokan (1974) and Anderson (1973). A match of the data curves to a model curve by shape alone yields the number of layers and their thicknesses and the ratio of the layer resistivities to ρ_1. The match of both abscissas and ordinates (ρ_a/ρ_1 and τ axes) allows two separate estimates of ρ_1, which completes the interpretation. Only the ρ_1 estimate from the τ-axis match is used here as the other is discussed with the asymptote evaluation method.

Out of 17 soundings, only 5 deviated noticeably from the halfspace model shape. Soundings 14, 15 and 16 suggested a shallow layer slightly more conductive than the halfspace below and 30 and 31 suggested a resistive surface layer with a more conductive halfspace below. Noting that $\rho = 1/\sigma$, the curve-match interpretations for layer thicknesses and conductivities are listed in Table II.

Asymptote Evaluation

The theoretical halfspace transient voltage response, expressed as equation II.11, can be approximated asymptotically in two different time ranges. For early times ($0 \leq t \leq 0.05 \frac{\mu_o r^2}{\rho}$), the voltage response is

approximately

$$\bar{v}(t) \cong \frac{3Iyn_t A}{2\pi r^5}\rho .$$

The equation becomes more exact the closer t is to zero. For late times ($1.1\frac{\mu_o r^2}{\rho} \leq t \leq 50\frac{\mu_o r^2}{\rho}$), the voltage response is approximately

$$\bar{v}(t) \cong \frac{n_t AIr\,\mu_o^{5/2}}{40\,\pi^{3/2}\rho^{3/2}}\, t^{-5/2}$$

(Silva, 1969, p. 37). By solving these two asymptotic expressions for ρ and observing how the resulting functions behave for an N-layered earth model (Jackson and Keller, 1972), we find that

$$\rho_1 \approx \frac{2\pi r^5}{3Iyn_t A}\bar{v}(t) \quad , \text{ if } 0 \leq t \leq 0.05\frac{\mu_o r^2}{\rho_1} \qquad \text{(IV.11)}$$

and $$\rho_N \approx \left(\frac{4n_t AIr}{5v(t)t^{5/2}}\ \pi x 10^{-17.5}\right)^{2/3} \quad , \text{ if}$$

$$1.1\frac{\mu_o r^2}{\rho_N} \leq t \leq 50\frac{\mu_o r^2}{\rho_N}. \qquad \text{(IV.12)}$$

Since we cannot presume ρ_1 or ρ_N, these two equations should be calculated for each sounding and plotted versus time. The resulting functions should approach constant-resistivity asymptotes when the respective time criterions are met.

Examples of these two functions are plotted in Figure 6 for sounding 5. None of the other plots of the data reduced by equation IV.11 are included because the curves are identical to those in Figure B.1 with the ordinate converted to resistivities by equation IV.10. The early-time asymptotes were evaluated and listed in Table II as conductivities. The late-time curves (data reduced by

Figure 6. A plot of the early and late time asymptotic expressions and their interpretations for sounding 5. Constant conductivity asymptotes of 0.10 mho/m for the early-time curve and 0.12 for the late-time curve have been picked.

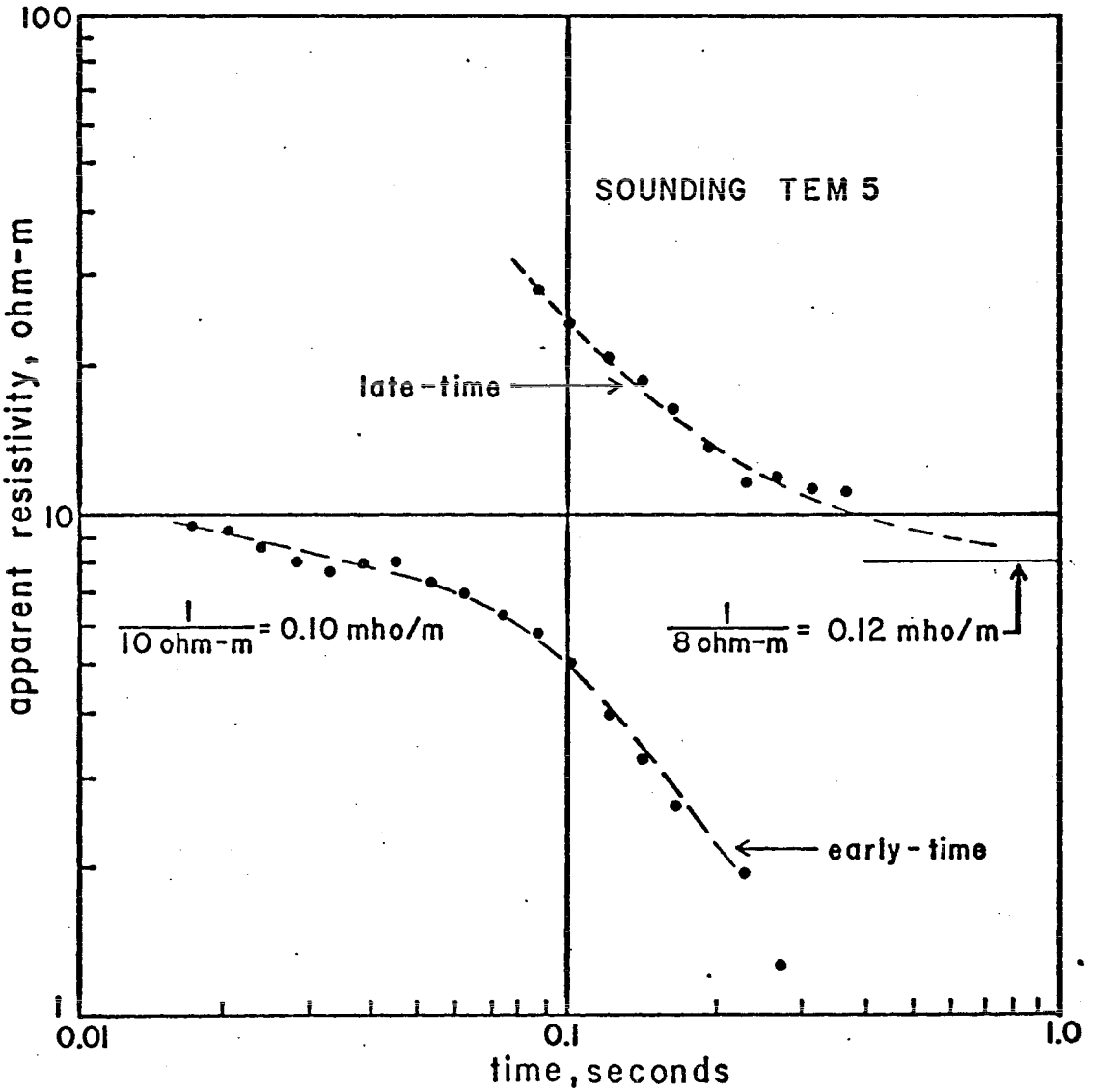

equation IV.12) are all plotted in Figure B.3. Strict evaluations were not possible for all the sounding data because only soundings 25, 26 and 29 were sampled at large enough times to satisfy the criterion in equation IV.12. Nevertheless, interpretations were attempted and are listed in Table II as conductivities.

Where the late-time curves showed deflections suggestive of two layers, extrapolations were made to determine the resistivities; the depths were approximated from models in Vanyan (1967). Soundings 1, 3, 23, 25, 28, 29, 30 and 31 show deflections which suggest a resistive basement 3 to 5 km deep. The depth to this basement is surprisingly large and exceeds the source-sensor separation for most of the soundings. The deflection in the late-time curves which indicate the existence of the basement corresponds to the smallest voltages in the data set and could be the result of insignificant voltage variations. Therefore, the complete interpretations are listed in Table II, but the resistive basement indications should be dismissed because they are too prone to error.

Estimation by Half-Amplitude Decay Time

This method (suggested by C. Zablocki, personal communication, 1974) is quite simple and can provide quick results in the field. It is only approximate, however, and is not recommended as a replacement for the more rigorous interpretational techniques. The basic principle of this method is that an "apparent conductivity" can be calculated from the time it takes the transient to decay to half its initial amplitude. Similar to the standard meaning of "apparent

conductivity," here it refers to the conductivity of a halfspace whose half-amplitude decay time, $t_{\frac{1}{2}}$, is equivalent to that observed. The halftime for a theoretical halfspace transient response (equation II.11) is given by

$$t_{\frac{1}{2}} = \frac{\mu_o r^2 \sigma}{2} 0.23 \ .$$

Solving for σ and labeling it as the apparent conductivity, σ_a, we find that

$$\sigma_a = 6.92 \times 10^6 \frac{t_{\frac{1}{2}}}{r^2} \ . \qquad \text{(IV.13)}$$

The apparent conductivity values as determined in the field for each sounding (Klein and Kauahikaua, 1975) are listed in Table II.

Evaluation and Comparison of the Interpretational Methods

The interpretational methods discussed here represent the four most-used techniques by which transient data can be interpreted. They differ from each other on three basic points. First, the use of partial inversion and curve-matching can provide full layering information whereas the other methods do not. Secondly, when using these two full information methods, partial inversion compares actual data and model values while curve-matching compares the logarithms of data and model values. Finally, although all four methods can determine the surface-layer conductivity by using the shape of the data curve, only partial inversion and asymptote evaluation allow an independent, surface-layer conductivity estimate by data amplitude as well. The following discussion and comparison of interpretational methods and

their results will be primarily on the basis of these differences.

Estimation by half-amplitude decay time is intended for obtaining approximate results in the field. The apparent conductivities that were calculated from the half-amplitude decay times of the Puna transient data rarely differed from other halfspace conductivity estimates by more than a factor of 1.5. Note that the estimation of the decay time depends only on its shape as a function of time and is independent of the transient's absolute amplitude. The accuracy of the apparent conductivity estimates in Puna stem from the fact that the transient responses observed there did not differ markedly from the shapes of halfspace responses. The technique would still yield good results for surveys over two-layer earths, but would require observing transients at many different spacings (e.g. apparent conductivities would be close to σ_1 for spacings which are small with respect to the thickness of the surface layer and would approach σ_2 for larger spacings). The accuracy of this method is rather surprising since the decay time was estimated from the transient data before it was compensated for the instrumentation effects. The distortion by the recording equipment seems to have had little effect on these decay times which suggests that estimation by half-amplitude decay time can be used as a field technique for the detection of conductivities at least in the range of 0.05 to 0.40 mho/m.

The asymptotic evaluation techniques were developed to discover subsurface layering parameters by manipulating the data to yield constant-resistivity asymptotes. The asymptotes are approached if the conditions of equations IV.11 and IV.12 are fulfilled. In Puna,

only a few of the early-time asymptotes and none of the late-time asymptotes were developed for the simple reason that, for the conditions encountered, the transients were not sampled over a wide enough range of times. The method was, therefore, of little use in Puna.

The early-time asymptote method is a straightforward determination of conductivity values by the larger, more well defined amplitudes of the early portion of the transient data curve. Note that the early-time asymptote expression is independent of time (equation IV.11). On the other hand, the late-time asymptote method (as with equation IV.12) utilizes both shape (dependent on time) and amplitude in the later portion of the data curve where the transient amplitudes can be quite small. The deflections in the Puna late-time curves (Figure B.3) which initially suggested a 3 to 5 km deep resistive basement were the result of very small amplitude variations in the data (usually less than 1% of the transient's maximum amplitude which is a variation one-tenth the noise amplitude for a noise ratio of 10) amplified through the use of equation IV.12. Although the late-time asymptote method is very promising for transient sounding, its results can be misleading if based on indiscriminate amplification of insignificant voltage variations. Ideal data for such an analysis would have a constant relative precision for each data point (e.g. a precision of 5%); otherwise, the results of the interpretation will require qualification, as did the Puna findings.

Logarithmic curve-matching also involves some manipulation of the smaller transient data values. With this method, the data and

model values are visually compared so as to minimize the logarithms of their ratios (see equation IV.1). The procedure does not discriminate between small amplitude values and large amplitude values. For example, model and data values of 1 and 2 volts or 1 and 2 mv, respectively, would be no worse matches than values of 1 and 2 μv by the logarithmic comparison criterion. If this range of amplitude values was actually represented in one data set and each had been measured with a precision of 10 μv (typical for the Puna transient data) for example, then this sort of logarithmic comparison becomes ludicrous. One should expect all data and model values to be within approximately 10 μv of each other for a good match. If each data value had been measured with a precision of 10% (typical for Schlumberger or frequency sounding data), for example, then use of the logarithmic comparison can be rationalized (see discussion on this point at the beginning of this chapter).

The Puna data were also interpreted by curve-matching for purely comparative purposes. Twelve of the seventeen transient responses appear to fit the halfspace model quite well while the other five fit models having thin surface layers of varying resistivity over halfspaces. The data points which are most indicative of the contrasting surface layer for the five soundings are always the earliest 2 to 5 points. Vanyan (1967, p. 201) points out that the earliest portion of the transient signal can be greatly distorted by experimental errors such as laying the measuring coil out on a sloping surface or at a different elevation from the current source so that the coil and current source are not coplanar. The early transient can also be

distorted by excessive filtering (Skokan, 1974). As with the interpretations by late-time asymptote evaluation, the suggestion of contrasting surface layers by these five soundings is not based on the most reliable data points and should be dismissed unless further evidence can be found.

One of the greatest advantages of using the partial inversion method over any of these other interpretational schemes is the capacity to test the goodness-of-fit of the model to the data by standard statistical means. Fifteen of the seventeen sets of sounding data were fitted adequately by a homogeneous earth response (equation IV.4). Furthermore, the two homogeneous earth conductivity estimates for each sounding (one by the data's shape as a function of time and one by the data's amplitude) were close enough to be considered identical for eleven of those fifteen soundings. The most significant differences between the data and the models were for the first few data points; however, they were not great enough to require using a more complicated model. The thin contrasting surface layers or deep resistive basements which were suggested as a result of using logarithmic curve-matching and asymptotic evaluation are correctly dismissed because of being based on insignificant data variations. The five soundings for which the two homogeneous earth conductivity estimates did not match (σ_{θ_2} was less than σ_{θ_3}) and the two soundings which were fit inadequately by the halfspace response are most likely the result of errors in measuring experimental parameters like current amplitudes or distances because of the consistency between σ_{θ_3} values for soundings in close proximity.

A look at the residuals from the two inadequately fit soundings did not suggest that a more complicated layered model would improve the fit. The lack of fit was perhaps because of the effects of excessive noise, experimental error or inadequacies of a layered model to fit the true structure.

The partial inversion method (or any statistical inversion method) can provide statistically significant layering information by a straightforward comparison of data and model values without artificial manipulation. The comparison criterion is completely general. On the other hand, the use of logarithmic curve-matching and asymptote evaluation implicitly assumes that all data samples have been measured with comparable relative precisions (e.g. a precision of 5%). The interpretational results of these two methods are not provided with objective uncertainty estimates or qualifications. Interpretation of transient data by these two methods alone could easily lead to erroneous results; thus, it appears that the use of such methods would best be limited to providing initial estimates ultimately leading to a general inversion.

Most of the results of the different methods do agree in assigning "normal" conductivities of about 0.10 to 0.16 mho/m to soundings 1, 3, 5, 6, 7, 26, 28, 30 and 31 and "anomalous" conductivities of 0.30 to 0.50 mho/m to soundings 14, 15, 16, 23 and 24. Sounding 29 showed the lowest conductivity value of 0.016 mho/m. These values are based on conductivity estimates by shape because they are more consistent than the estimates by amplitude.

V. GEOELECTRIC STRUCTURE AND GEOLOGICAL IMPLICATIONS

The results of the transient soundings in east Puna show that the subsurface responds electrically as a homogeneous halfspace with "normal" conductivities of 0.10 to 0.16 mho/m for soundings 1, 3, 5, 6, 7, 26, 28, 30 and 31 and "anomalous" conductivities of 0.30 to 0.50 mho/m for soundings 14, 15, 16, 23 and 24. Sounding 29, the only one northwest of the rift zone, responded as a halfspace with a low conductivity of 0.016 mho/m. In totally saturated rocks, the bulk rock conductivity can be described in terms of the average porosity fraction, ϕ, and the pore water conductivity, σ_ω, by the empirical relationship

$$\sigma = G \sigma_\omega \phi^m \qquad (V.1)$$

where σ is the bulk rock conductivity and G and m are empirically determined constants (Keller and Frischknecht, 1966). For Hawaiian basalts, Keller (1973) and Manghnani et al. (1976) have calculated (G,m) to be about (0.29, 1.8), respectively. Using this relationship for a porosity of about 25% (a reasonable average for surface lavas from Zablocki et al., 1974) and the normal bulk conductivities of 0.10 to 0.16 mho/m, we find that the pore water conductivity is about 4 to 6 mho/m. For the anomalous bulk conductivities of 0.30 to 0.50 mho/m, we determine the pore water conductivity to be about 13 to 21 mho/m.

The normal values of 4 to 6 mho/m are much too high for fresh water but correspond closely to those for normal seawater at 20° C

(5 to 6 mho/m from Schlichter and Telkes, 1942). This is not surprising because seawater underlies the whole area at depths greater than a few hundred meters. Fresh water, if present, forms a thin layer floating upon the seawater. Dry lavas as well as lavas saturated with fresh water would be several times more resistive than the lavas saturated with seawater below, and are apparently not delineated by these transient soundings.

The higher pore water conductivity values of 13 to 21 mho/m may indicate seawater at temperatures higher than 20° C. According to Dakhnov (1962), the conductivity of a fluid at a temperature T, $\sigma_\omega(T)$, is related to its conductivity at 18° C, $\sigma_\omega(18°\ C)$, by

$$\sigma_\omega(T) = \sigma_\omega(18°C)\left[1 + \alpha(T - 18°C)\right] \qquad (V.2)$$

where α is the temperature coefficient of conductivity (generally taken as 0.025/°C). Comparison with the data of Quist and Marshall (1968) confirms that the relationship is valid for temperatures from 18° C to 250° C. If $\sigma_\omega(18°\ C)$ is taken to be 5 mho/m, then 13 to 21 mho/m corresponds to temperatures of about 82° to 146° C.

The anomalously low bulk conductivity of 0.016 mho/m for sounding 29 northwest of the rift corresponds (by equation V.1) to pore water with a conductivity of 0.67 mho/m. This is much too low for seawater except at near freezing temperatures, so the pore waters must be less saline than seawater and are probably at normal temperatures. Pore water conductivity increases nearly linearly with

salinity and is approximated by

$$\sigma_\omega \propto S^{0.916} \qquad (V.3)$$

where S is the pore water salinity in ppt (parts per thousand) (Logan, 1961). Using the fact that seawater has a salinity of 35 ppt, water of conductivity 0.67 mho/m must have a salinity of about 3.9 ppt.

Figure 3 shows the locations of the sensor coils and current sources for each of the 17 transient soundings. The anomalous conductivity estimates (from soundings 14, 15, 16, 23 and 24) are confined to a 30 or 40 km^2 area south of the rift between Puu Honuaula and Kapoho Crater. Soundings 3 and 5 do not fit this generalization although they are included in the anomalous area in close association with sounding 15. For such an area where there are lateral changes in earth conductivity, it is important to know the region of greatest influence on the observed signal at each sounding location. Vanyan (1967, p. 70) plots his interpretations at the point midway between source and sensor for unstated reasons. Model studies over a conducting cylinder (Wait and Hill, 1973) show that the effect of the lateral conductivity variation is a maximum when the cylinder is between the sensor coil and the midpoint. It is probably more reasonable to plot the Puna conductivity estimates at each sounding configuration midpoint rather than at the source or sensor location. The resulting map was so contoured (Figure 7) and the anomalous area is apparent as the group of conductivity estimates which exceed 0.3 mho/m.

Table II. Summary of transient sounding interpretations. All numbers refer to estimates of σ_1 unless noted otherwise.

Sounding	PARTIAL INVERSION σ_{θ_2}	PARTIAL INVERSION σ_{θ_3}	$F(\vec{\theta})$	σ_{θ}	CURVE-MATCH			ASYMPTOTE EVALUATION Early	Late		
1	.142 ± .3200	.161 ± .020000	1.091	.25	.15			.15	.17	$\sigma_2 \leq .10$	d≈4300
3	.119 ± .0066	.111 ± .000028	1.089	.12	.09			.11	.09	$\sigma_2 \leq .05$	d≈5000
5	.089 ± .0075	.113 ± .000036	1.100	.14	.10			.10	.12		
6	.156 ± .0650	.142 ± .002900	1.092	.08	.15			.14	.15		
7	.116 ± .0270	.121 ± .000470	1.140	.13	.08			.09	.20		
14	.266 ± .0230	.327 ± .000170	1.086	.27	.38	$\sigma_2 \leq .32$	d≤60	.22	.30		
15	.016 ± .0250	.473 ± .000670	2.150	.20	.50	$\sigma_2 = .43$	d≤50	.10	.50		
16	.147 ± .2800	.308 ± .000330	1.100	.21	.46	$\sigma_2 = .14$	d=390	.14	.40		
23	.306 ± .0450	.301 ± .000120	1.070	.36	.26			.71	.33	$\sigma_2 \leq .10$	d≈3300
24	.145 ± .2300	.335 ± .009900	1.094	.29	.34			.23	.40		
25	.127 ± .0160	.054 ± .000013	2.570	.17	.04			.08	.10	$\sigma_2 \leq .03$	d≈4300
26	.068 ± .0160	.116 ± .000072	.810	.16	.07			.09	.10		
27	.075 ± .0110	.159 ± .000100	1.074	.15	.16			.07	.17		
28	.063 ± .0150	.105 ± .000061	.970	.11	.08			.07	.16	$\sigma_2 \leq .01$	d≈4500
29	.009 ± .0420	.016 ± .000022	1.040	.06	.02			.02	.03	$\sigma_2 \neq .02$	d≈4500
30	.091 ± .0370	.101 ± .003000	.360	.10	.00	$\sigma_2 = .08$	d≤450	.06	.09	$\sigma_2 \leq .02$	d≈4500
31	.103 ± .2700	.118 ± .057000	.988	.18	.00	$\sigma_2 = .12$	d≤185	.08	.14	$\sigma_2 \leq .02$	d≈4500

Definition of the parameters.

$\sigma_{\theta_2}, \sigma_{\theta_3}$: estimates by amplitude and shape, respectively, from partial inversion.

$F(\vec{\theta})$: F-statistic of inversion by which σ_{θ_2} and σ_{θ_3} were estimated.

σ_2, d : parameters of two-layer interpretation. σ_2 is conductivity of deepest material and d is the depth to it.

The depth of resolution (the depth range represented by the interpreted conductivities) for transient sounding has not yet been determined precisely from theory. It can, however, be determined qualitatively from model studies. For example, frequency response models (Frischknecht, 1967) and transient response models (Silva, 1969) for a horizontal coil and current source over a two-layer earth show conclusively that the response is not appreciably different from a halfspace response with a conductivity of the first layer if the second layer is generally at depths greater than r/3. A perfectly resistive second layer can be detected if it is shallower than r/2 and a perfectly conductive second layer can be detected shallower than 3r/4. The limiting, or maximum depth of resolution is independent of the source-sensor separation, r, and is equal to a skin depth, δ (Mundry, 1966). In specific terms for Puna, the maximum skin depths of 0.1 to 0.5 mho/m material using the frequencies from 1 to 35 Hz (as was done in this survey, see chapter III) are 4500 and 2000 m, respectively. The actual depths of resolution achieved by transient soundings were not nearly this large and did not exceed 1500 m (assuming that we are not looking for perfect conductors or resistors) owing to the small source-sensor separations. Mundry (1966) also points out that if the surface layer of a two-layer model is thinner than $\delta/16$, then the response will not be appreciably different from that of a halfspace with the conductivity of the second layer. This explains why the resistive material above sea level (conductivities less than 0.0015 mho/m) in Puna was far less apparent from the transient sounding results than it was from

the results of direct-current soundings (Klein and Kauahikaua, 1975 and Keller, 1973).

The transient sounding results from east Puna show that sub-sea level conductivities correspond to water saturated basaltic lavas which vary laterally reaching a maximum south of Puu Honuaula. Vertical changes by a factor of 10 in conductivity can be ruled out by the data at least to depths approaching 1 km below sea level. The lateral conductivity variation is interpreted to indicate temperature variation to a maximum of 150° C. The area of anomalous temperature is partly outlined in Figure 7 by the 0.3 mho/m contour and is the same area where coastal springs and well waters off the rift are the warmest (see Figure 1). The groundwater has apparently been disturbed by these thermal effects because no Ghyben-Herzberg lens exists there. Coverage of the rift trace and adjacent areas by transient soundings was insufficient to fully outline the thermally disturbed zone, but it appears to be distinct from the rift structure at depths above 1 km below sea level. There are several possibilities for the location of the heat source; however, the transient sounding results are inconclusive on this point and any further discussion would be speculative.

Comparison of these results with the bipole mapping results of Keller (1973) and the transient sounding results of Skokan (1974) in east Puna allow some generalizations to be made about the two methods and the basic structure in Puna. The transient sounding results in this study and those in Skokan's study are difficult to compare because they cover mutually exclusive areas (this study

covers the areas south and east of the Skokan area) and because they were interpreted with different techniques. Skokan interpreted her data by a variant of the logarithmic curve-matching interpretative technique which yielded as many as three layers with the last layer deeper than the r/3 limit discussed above. In light of the discussion on practical limitations of transient sounding, an interpretation of this complexity is difficult to justify. If we omit any structure from her interpretations that is deeper than 1500 m (maximum r/3) and view the surface-layer conductivity interpretations only as possible maximums, her results reduce to no more than two layers and are in fact very similar to those normal values from the present study. With these modifications, her conductivities never exceed 0.3 mho/m. The rift trace appears as a less conductive zone bordered by broad areas with conductivities of about 0.1 to 0.2 mho/m in both the transient sounding and bipole mapping studies. The anomalous zone outlined by this transient sounding study is not covered sufficiently by bipole mapping results to be verified, but apparent conductivities as high as 0.45 mho/m were observed within the zone.

The transient studies appear to be relatively unaffected by lateral conductivity changes when compared with the bipole mapping studies. The strong correlation between bipole apparent conductivities and transient sounding surface layer conductivity indications (Skokan, 1974) suggests that the bipole method achieves a penetration of perhaps a few hundred meters where there are lateral conductivity variations near the surface. Transient sounding, on the other hand, is more sensitive to the conductivities at greater depths.

Figure 7. A map of the study area with the interpreted conductivities for each sounding plotted at the midpoint between source and sensor. The values are in mho/m and the contour interval is 0.15 mho/m.

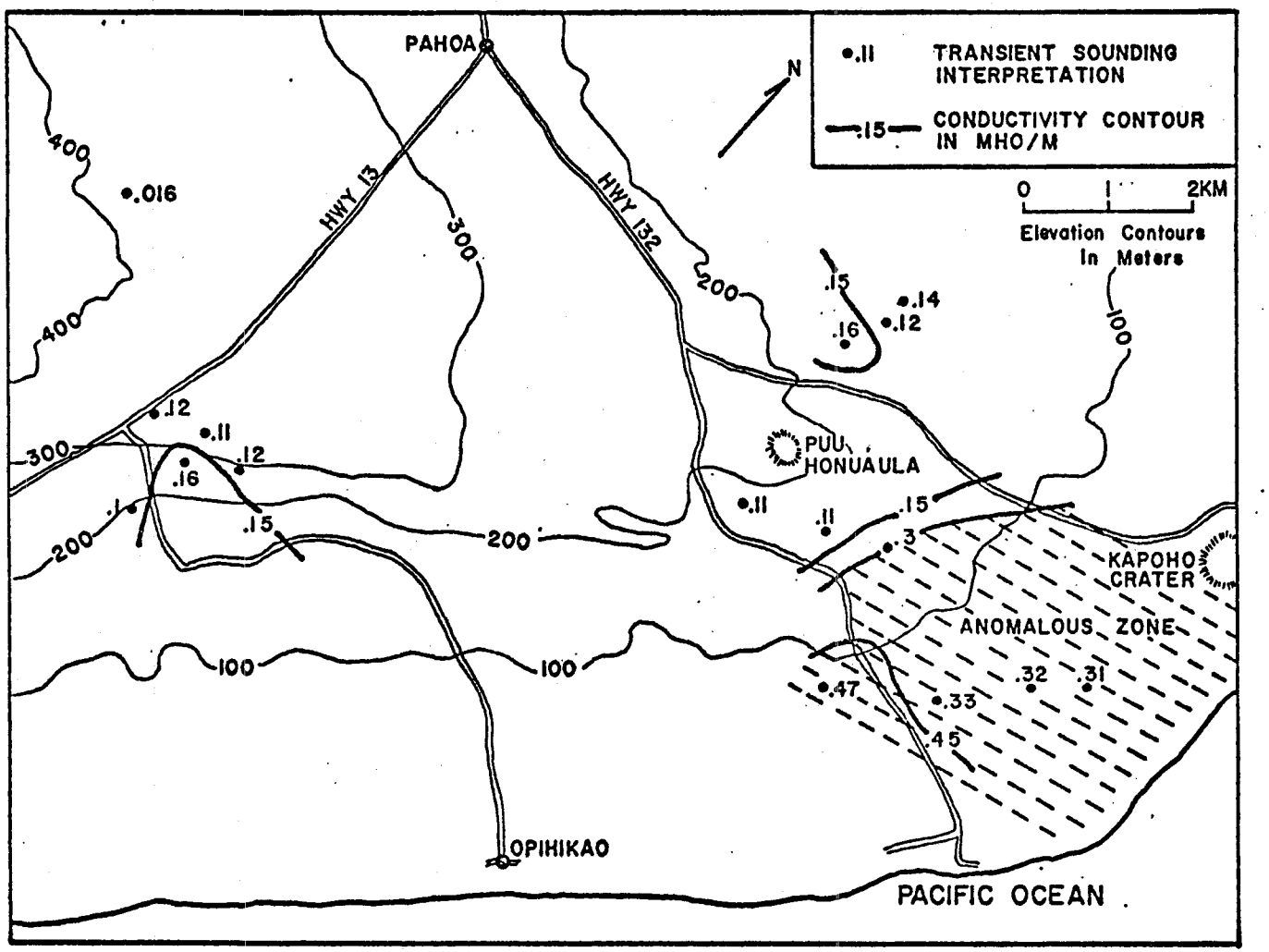
PAHOA
N
.11 TRANSIENT SOUNDING INTERPRETATION
.15 CONDUCTIVITY CONTOUR IN MHO/M
0 1 2KM
Elevation Contours In Meters
HWY 13
HWY 132
400
300
200
100
.016
.12
.11
.16
.15
.14
PUU HONUAULA
KAPOHO CRATER
ANOMALOUS ZONE
.32
.31
.47
.33
.45
OPIHIKAO
PACIFIC OCEAN

VI. CONCLUSIONS

A. Interpretative techniques based on inversion or non-linear regression are completely general and should be used with transient sounding data because they do not presuppose anything about the data. Curve-matching or asymptote evaluation can be used, but they are only recommended as a preliminary to an inversion technique because they tend to emphasize particular sections of the data without regard to data precision (depending on the method) and can easily lead to erroneous conclusions.

B. From the present results, Puna appears to be uniform vertically to a depth of about 1000 m below sea level and shows broad, but distinct, lateral conductivity variations. An area of anomalously high conductivities is delineated south of the rift at Puu Honuaula which is distinct from the rift zone (see Figure 7).

C. The anomalous conductivities discovered in Puna indicate maximum temperatures of 150° C. Transient sounding must be termed a potentially useful technique for geothermal exploration until these findings can be tested with a drilling program in the anomalous zone.

APPENDIX A: Fields About a Finite-Length Horizontal Current Source

The theory presented in chapter II is strictly valid for ideal dipolar antennas of infinitesimal dimensions. However, the large dipole moments required in geophysical applications can only be achieved by the use of a wire for a horizontal electric dipole whose length may be quite large with respect to the separation between source and observation point. Keller and Frischknecht (1966) and Wait (1954) show that a length of wire or a wire square will appear as infinitesimal dipoles with an error of less than 5% if the observation point is separated from the source by a distance of at least five times the maximum dimension of either the source or sensor. In practice, measurements are often taken at points much closer than this limit. Appropriate models for a horizontal current source may be calculated either by integration of the dipole field equations along the length of the current source (Scriba, 1974), or by the use of image theory (Kraichman, 1970). There are problems in both approaches: the integrations are generally not easily expressed in closed form except for the case of the direct-current electric fields, and image theory solutions are of uncertain validity (Wait and Spies, 1969). Therefore, the theory here is limited to homogeneous earth transient responses, and the integrations were performed numerically.

The integration for the transient response of the vertical magnetic field,

$$\frac{\partial}{\partial t} b_z(t)^{fin} = \frac{3I\rho y}{2\pi} \int_{x-\ell/2}^{x+\ell/2} \left[erf(u) - \frac{2}{\sqrt{\pi}}(u + \frac{2}{3}u^3)e^{-u^2} \right] \frac{dx}{r^5} \qquad (A.1)$$

(from equation II.10), is rather difficult to compute analytically, so the finite response was calculated as the sum of the responses from several shorter sources (whose total length was still ℓ). Each short source requires a unique separation and orientation angle (the program, FINITE, is listed in Appendix C). Calculations showed that this algorithm produced results which were accurate to within 1% when compared with theoretical results at large separations if each short source was less than one-fifth the separation. Several such responses are presented in Figure A.2 for a few values of r/ℓ and $\cos^{-1}(y/r)$.

The distortion is evident in the early portions of the transient, but becomes less noticeable as time increases. There would therefore be inaccuracies introduced into halfspace resistivity interpretation by curve-matching and early-time asymptote evaluation, but not by late-time asymptote evaluation as a result of measurements taken too close to a finite-length source but treated as a dipole field. To estimate these inaccuracies quantitatively, the apparent resistivity for the transients in Figure A.2 were determined by their early-time values and curve-matching (see chapter IV on interpretation), divided by the actual resistivity and plotted versus separation to source-length ratio (Figure A.1). The discrepancies can be surprisingly large and are greater than 5% for separations less than three times the source length. The effects are systematic; if the early

resistivity values overestimate the resistivity, curve-matching will underestimate it, and vice-versa. Constraining the resistivities obtained from transient amplitude and shape for measurements taken at distances less than three times the source length, as was done by Skokan (1974), will most certainly lead to erroneous interpretations.

An interesting result of these model studies is that the finite source effects discussed above may be minimized by measuring along particular source-receiver azimuths. For vertical magnetic field transient sounding this direction is approximately 70°. Figure A.1 shows that soundings with source and receiver separations as small as one source length along the 70° direction show no more than 6% amplitude error.

Figure A.1. Effects upon transient sounding interpretation for measurements taken close to a source. The figures show the results of interpretation attempts by curve-matching and asymptote evaluation on the transient models in Figure A.2.

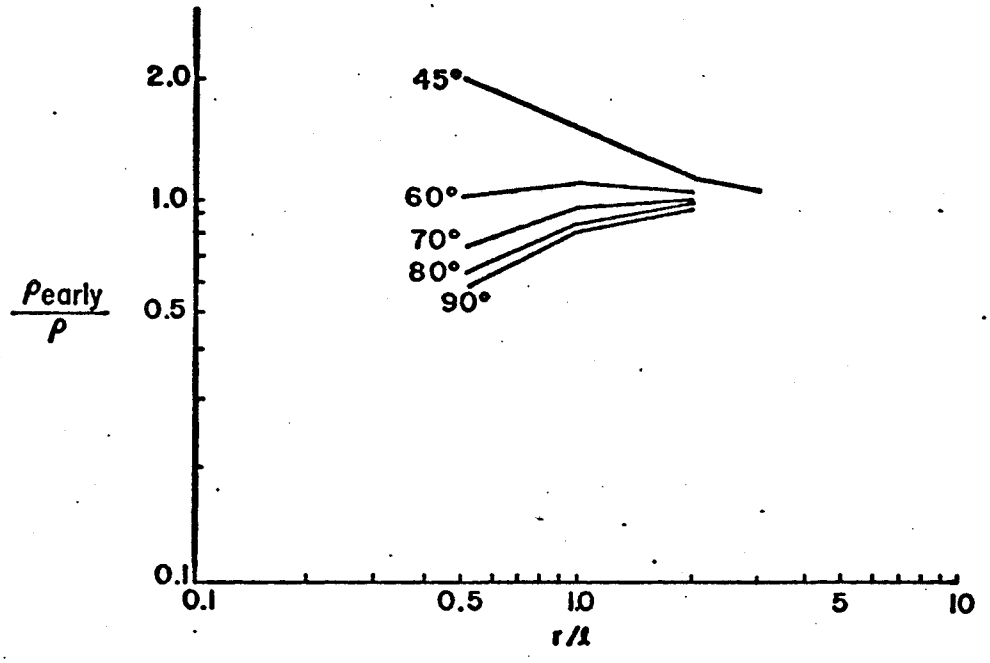
2.0
1.0
0.5
0.1
45°
60°
70°
80°
90°
ρearly / ρ
0.1
0.5
1.0
5
10
r/ℓ

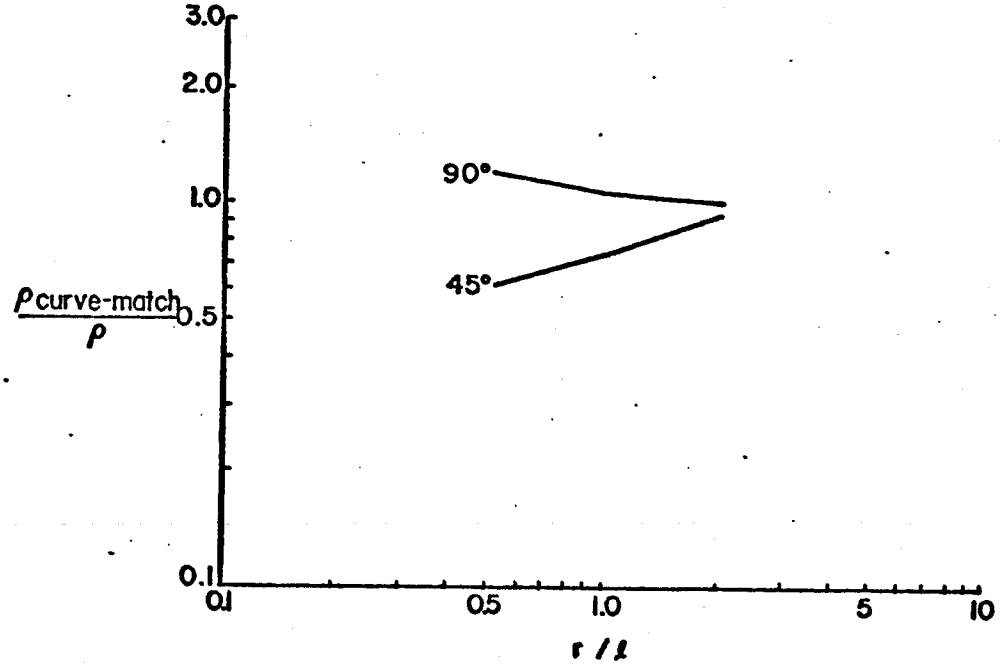
3.0
2.0
1.0
0.5
0.1
90°
45°
ρcurve-match / ρ
0.1
0.5
1.0
5
10
r / ℓ

Figure A.2. The transient response of the vertical magnetic field observed over a conductive halfspace close to a horizontal current source of length ℓ.

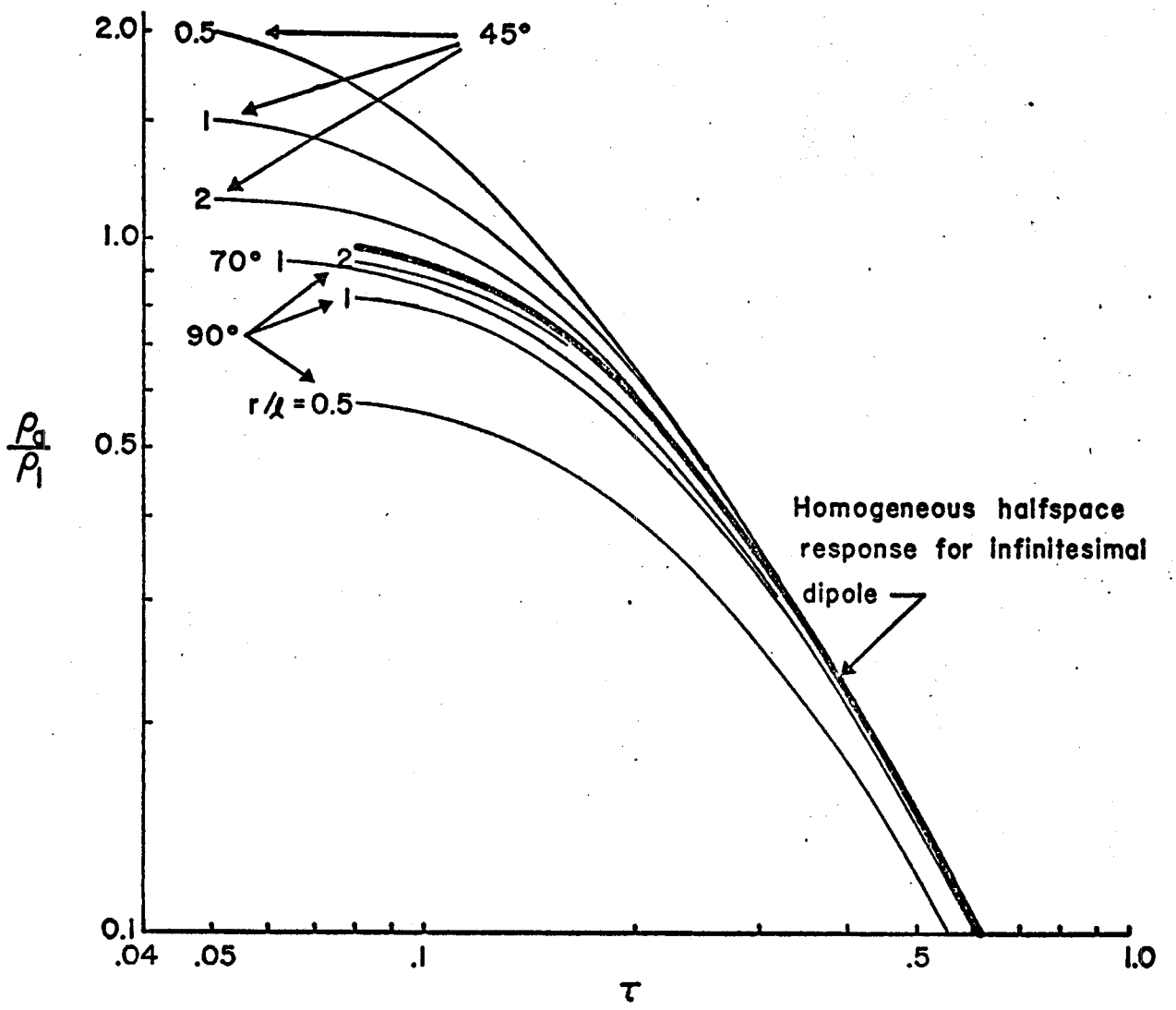
2.0
1.0
0.5
0.1
$\frac{\rho_a}{\rho_1}$
0.5
1
2
45°
70°
1
2
90°
1
r/ℓ = 0.5
Homogeneous halfspace
response for infinitesimal
dipole
.04
.05
.1
.5
1.0
τ

APPENDIX B: Transient Data Plots

Figure B.1. The transient sounding data for 17 locations. The actual voltages are plotted versus time along with the best-fit halfspace transient response. The procedure for obtaining the best-fit response is outlined in the text. The parameter correlation matrices are included.

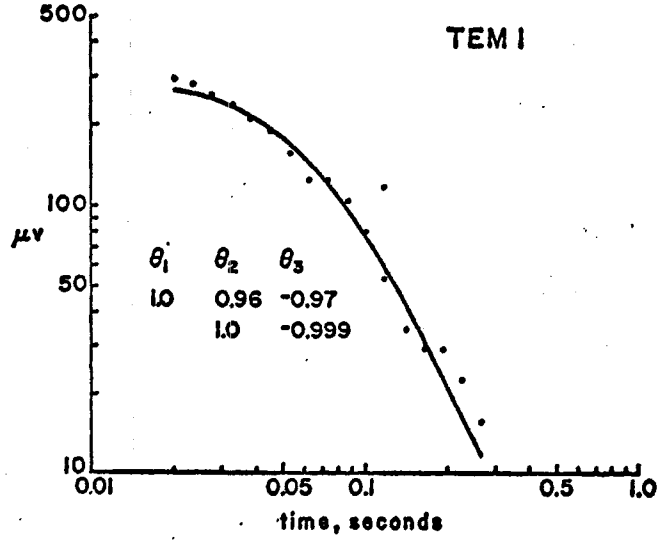
TEM 1
500
100
50
10
μv
θ1 θ2 θ3
1.0 0.96 -0.97
1.0 -0.999
0.01
0.05
0.1
0.5
1.0
time, seconds

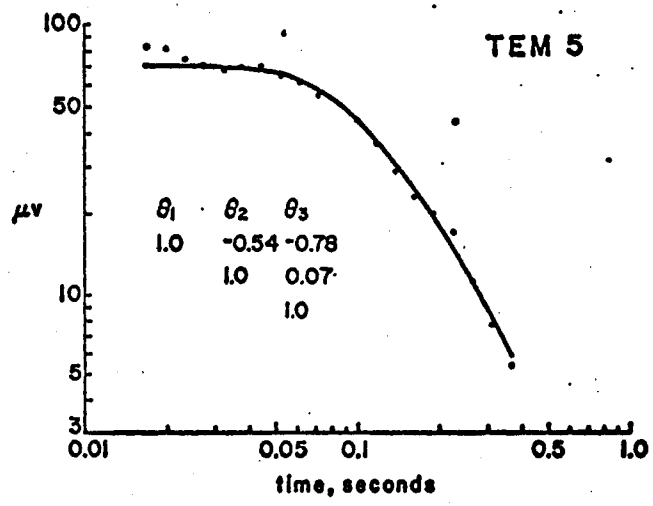
TEM 5
100
50
10
5
3
μv
θ1 θ2 θ3
1.0 -0.54 -0.78
1.0 0.07
1.0
0.01
0.05
0.1
0.5
1.0
time, seconds

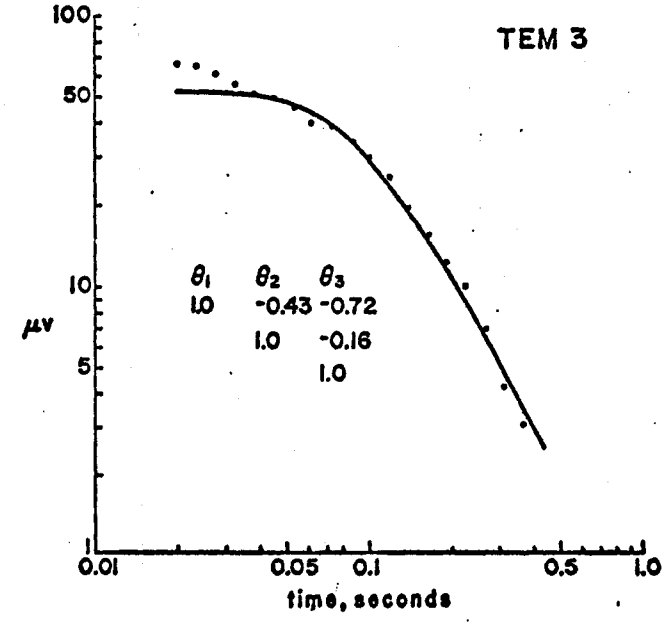
TEM 3
100
50
10
5
1
μv
θ1 θ2 θ3
1.0 -0.43 -0.72
1.0 -0.16
1.0
0.01
0.05
0.1
0.5
1.0
time, seconds

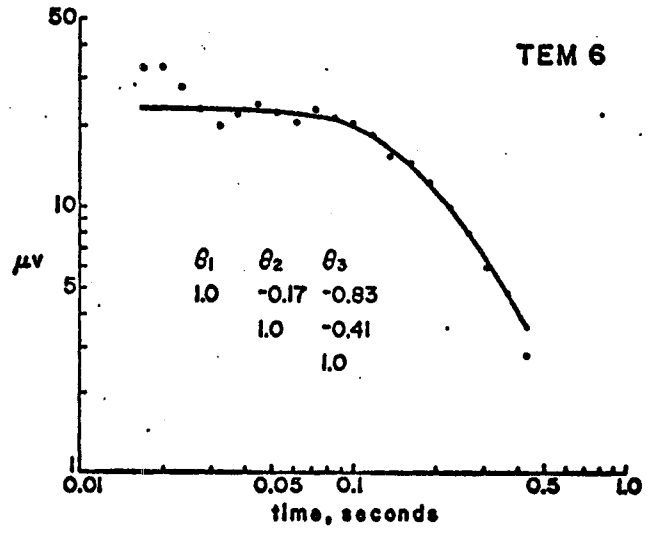
TEM 6
50
10
5
1
μv
θ1 θ2 θ3
1.0 -0.17 -0.83
1.0 -0.41
1.0
0.01
0.05
0.1
0.5
1.0
time, seconds

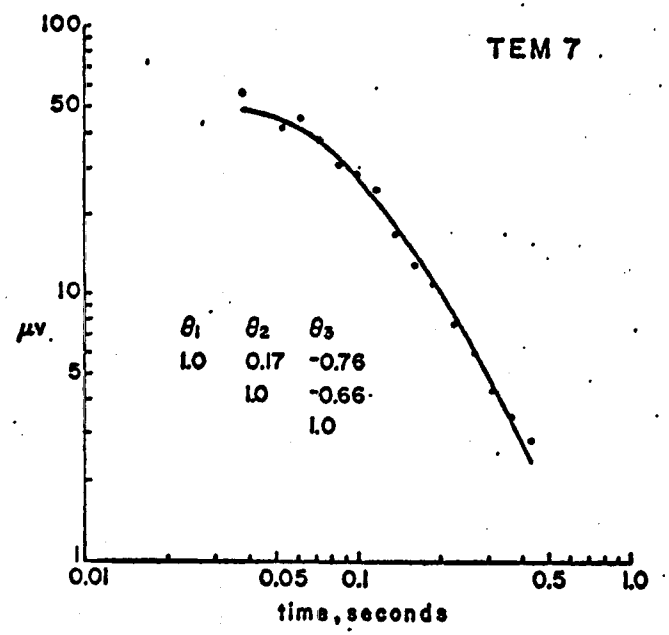
TEM 7
100
50
10
5
1
μv
θ1 θ2 θ3
1.0 0.17 -0.76
1.0 -0.66
1.0
0.01
0.05
0.1
0.5
1.0
time, seconds

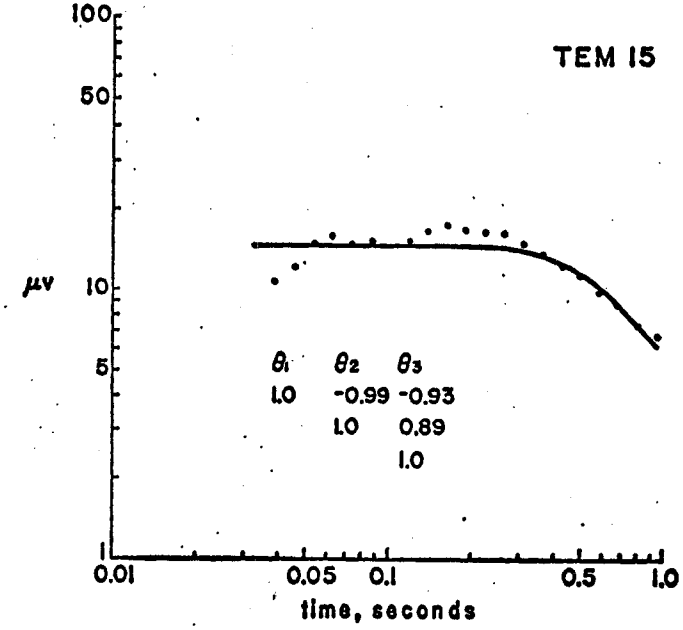
TEM 15
100
50
10
5
1
μv
θ1 θ2 θ3
1.0 -0.99 -0.93
1.0 0.89
1.0
0.01
0.05
0.1
0.5
1.0
time, seconds

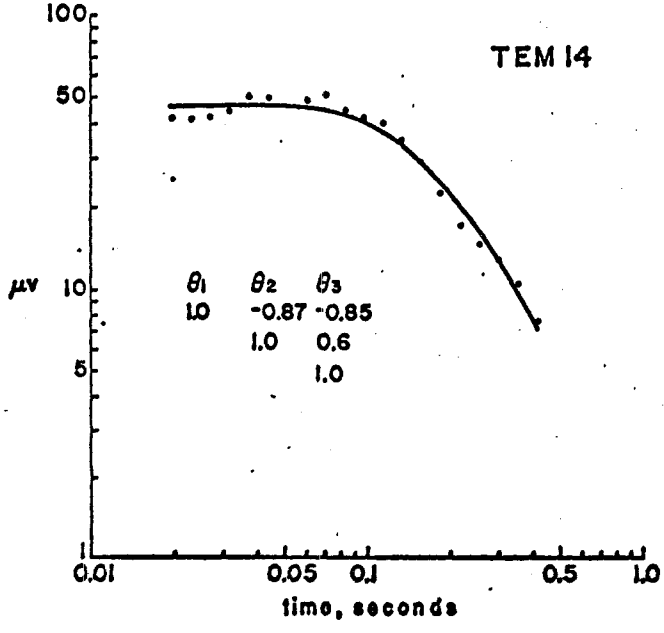
TEM 14
100
50
10
5
1
μv
θ1 θ2 θ3
1.0 -0.87 -0.85
1.0 0.6
1.0
0.01
0.05
0.1
0.5
1.0
time, seconds

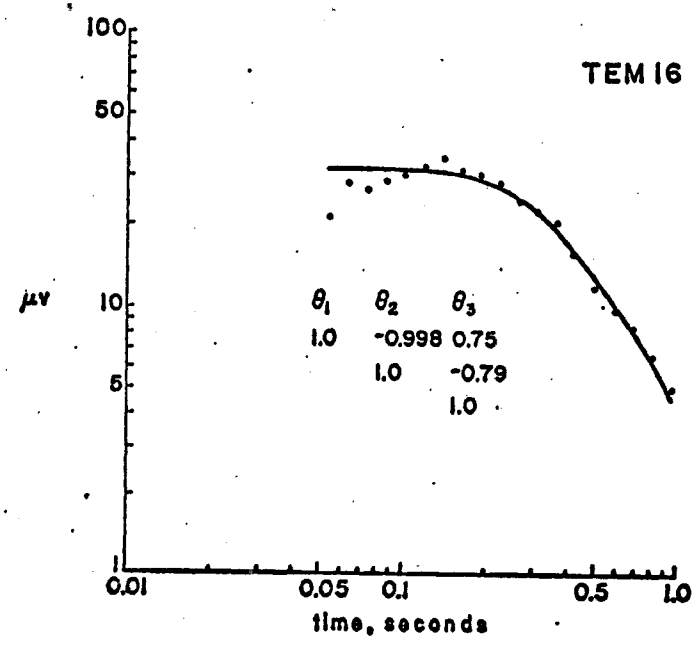
TEM 16
100
50
10
5
1
μv
θ1 θ2 θ3
1.0 -0.998 0.75
1.0 -0.79
1.0
0.01
0.05
0.1
0.5
1.0
time, seconds

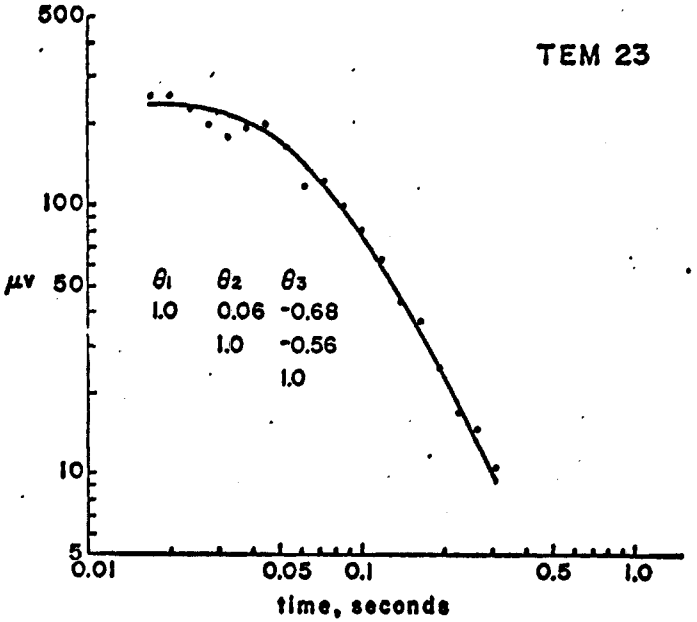
TEM 23
500
100
50
10
5
μv
θ1 θ2 θ3
1.0 0.06 -0.68
1.0 -0.56
1.0
0.01
0.05
0.1
0.5
1.0
time, seconds

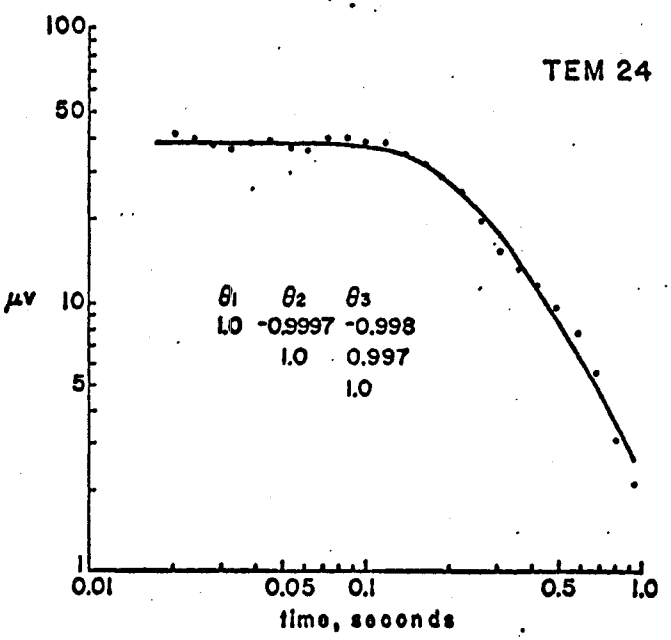
TEM 24
100
50
10
5
1
μv
θ1 θ2 θ3
1.0 -0.9997 -0.998
1.0 0.997
1.0
0.01
0.05
0.1
0.5
1.0
time, seconds

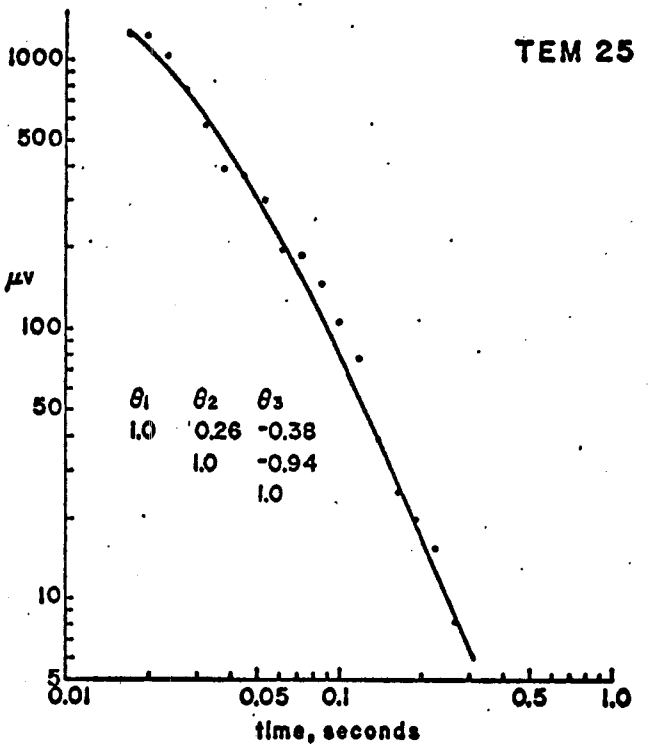
TEM 25
1000
500
100
50
10
5
μv
θ1 θ2 θ3
1.0 0.26 -0.38
1.0 -0.94
1.0
0.01
0.05
0.1
0.5
1.0
time, seconds

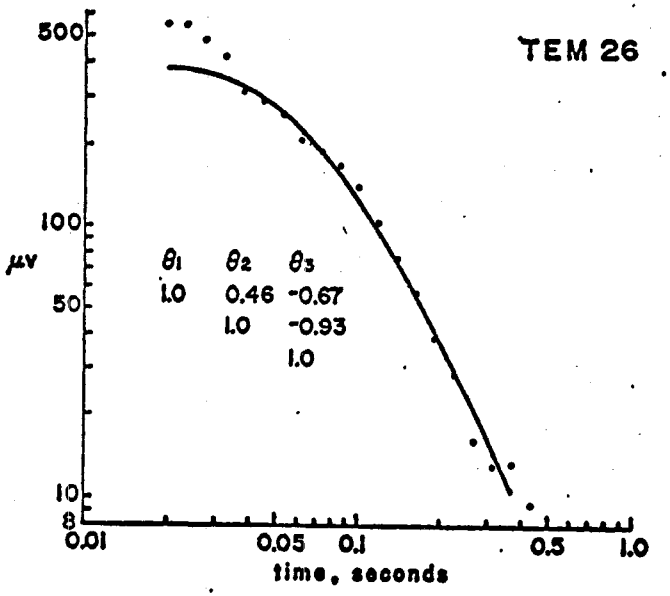
TEM 26
500
100
50
10
8
μv
θ1 θ2 θ3
1.0 0.46 -0.67
1.0 -0.93
1.0
0.01
0.05
0.1
0.5
1.0
time, seconds

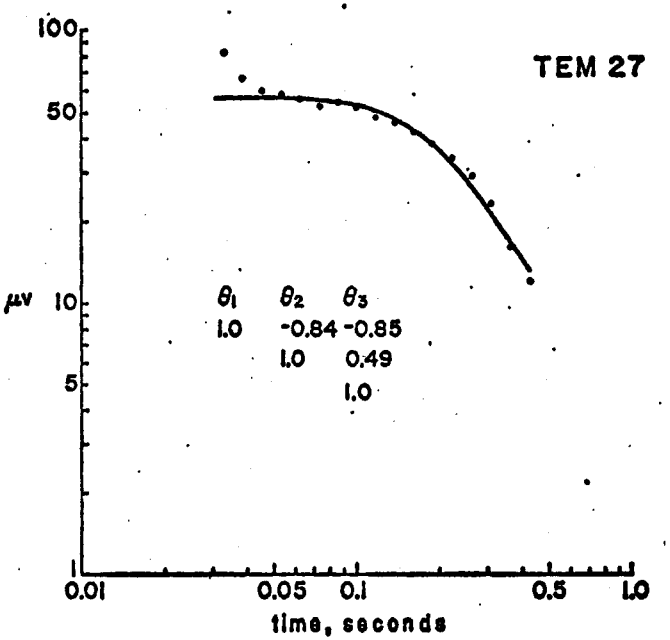
TEM 27
100
50
10
5
1
μv
θ1 θ2 θ3
1.0 -0.84 -0.85
1.0 0.49
1.0
0.01
0.05
0.1
0.5
1.0
time, seconds

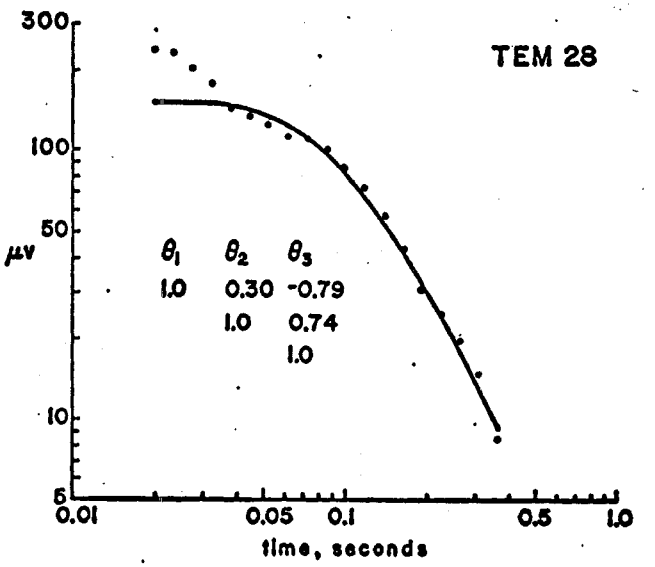
TEM 28
300
100
50
10
5
μv
θ1 θ2 θ3
1.0 0.30 -0.79
1.0 0.74
1.0
0.01
0.05
0.1
0.5
1.0
time, seconds

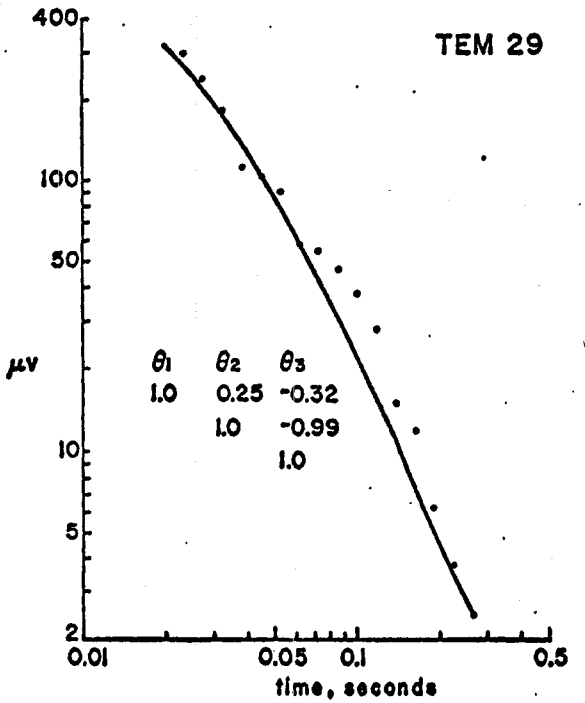
TEM 29
400
100
50
10
5
2
μv
θ1 θ2 θ3
1.0 0.25 -0.32
1.0 -0.99
1.0
0.01
0.05
0.1
0.5
time, seconds

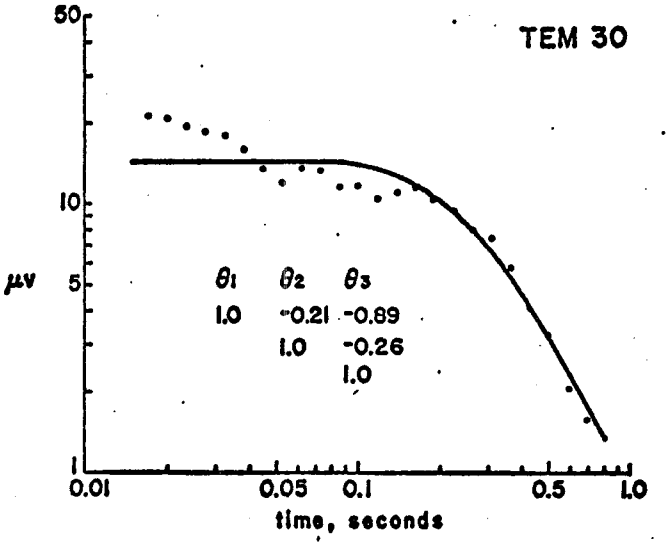
TEM 30
50
10
5
1
μv
θ1 θ2 θ3
1.0 -0.21 -0.89
1.0 -0.26
1.0
0.01
0.05
0.1
0.5
1.0
time, seconds

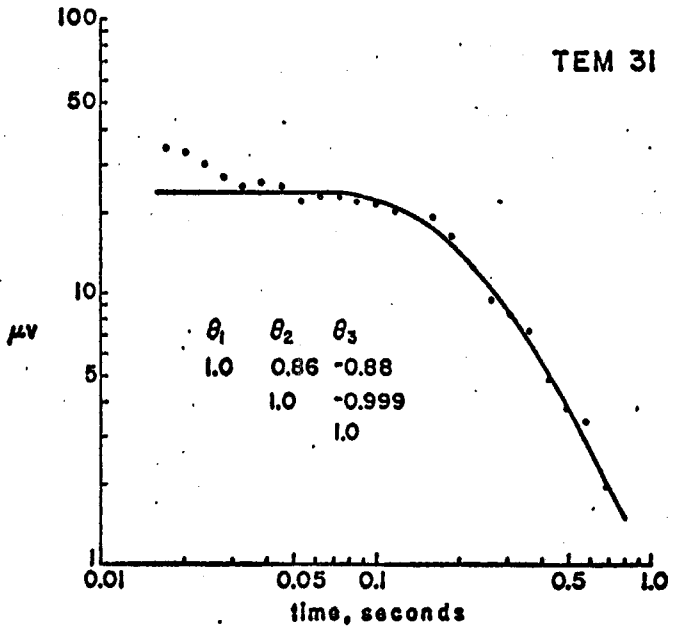
TEM 31
100
50
10
5
1
μv
θ1 θ2 θ3
1.0 0.86 -0.88
1.0 -0.999
1.0
0.01
0.05
0.1
0.5
1.0
time, seconds

Figure B.2. The data residuals (best-fit halfspace response subtracted from the data) plotted versus time. The ordinate in all plots is the residual amplitude divided by $\hat{\theta}_2$.

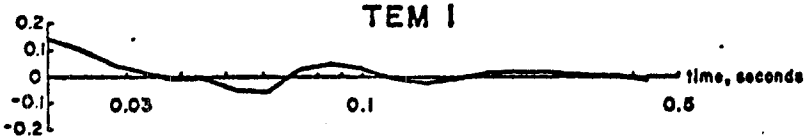
TEM 1
0.2
0.1
0
-0.1
-0.2
0.03
0.1
0.5
time, seconds

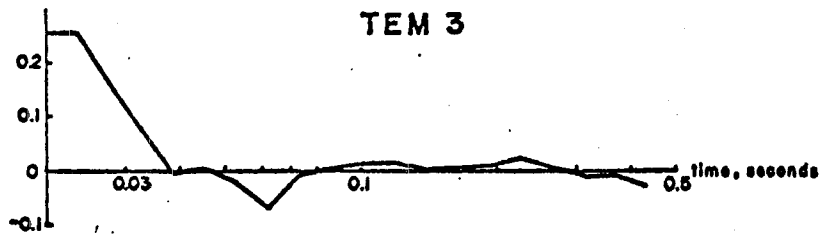
TEM 3
0.2
0.1
0
-0.1
0.03
0.1
0.5
time, seconds

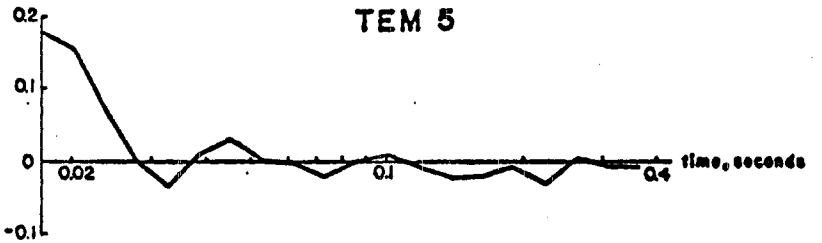
TEM 5
0.2
0.1
0
-0.1
0.02
0.1
0.4
time, seconds

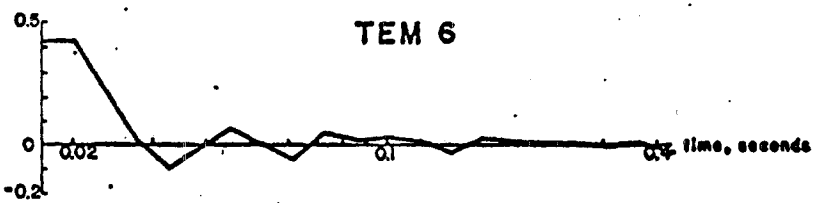
TEM 6
0.5
0
-0.2
0.02
0.1
time, seconds

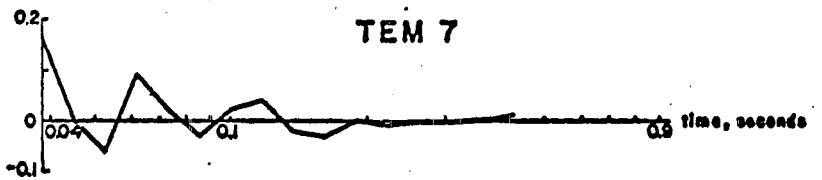
TEM 7
0.2
0
-0.1
0.04
0.1
time, seconds

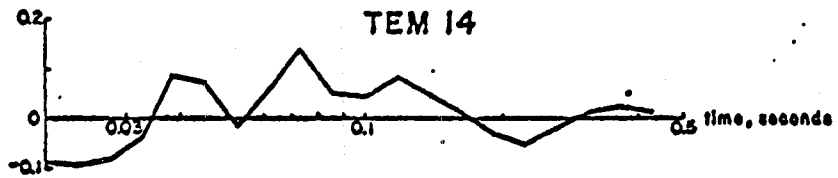
TEM 14
0.2
0
-0.1
0.05
0.1
0.5
time, seconds

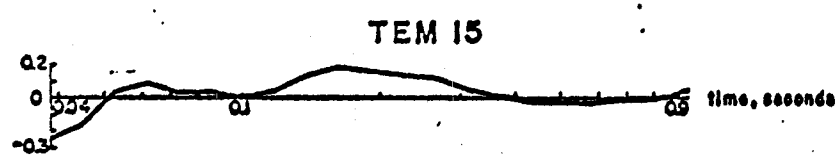
TEM 15
0.2
0
-0.3
0.04
0.1
0.5
time, seconds

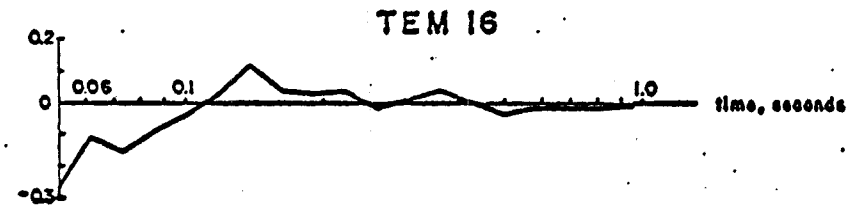
TEM 16
0.2
0
-0.3
0.06
0.1
1.0
time, seconds

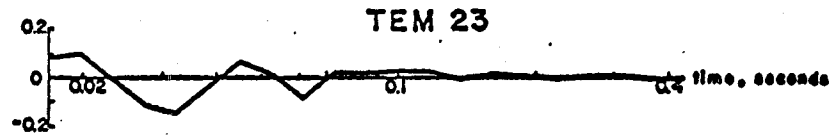
TEM 23
0.2
0
-0.2
0.02
0.1
0.4
time, seconds

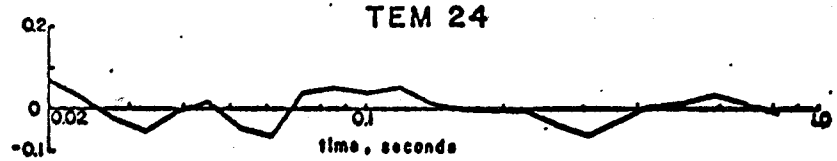
TEM 24
0.2
0
-0.1
0.02
0.1
time, seconds

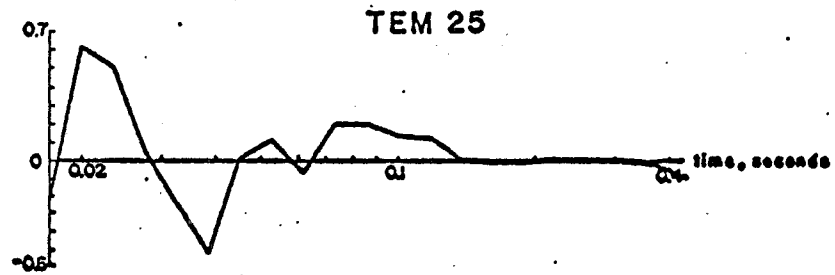
TEM 25
0.7
0
-0.5
0.02
0.1
time, seconds

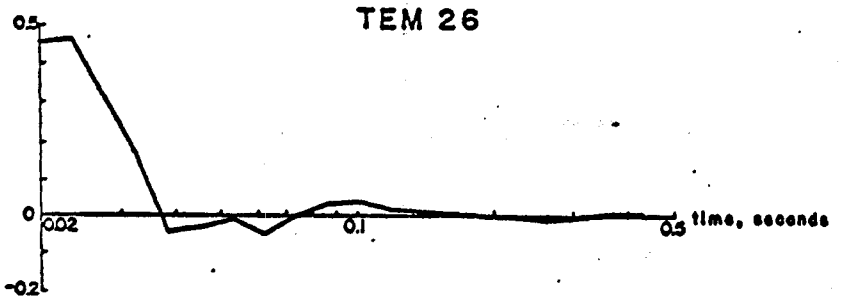
TEM 26
0.5
0
-0.2
0.02
0.1
0.5
time, seconds

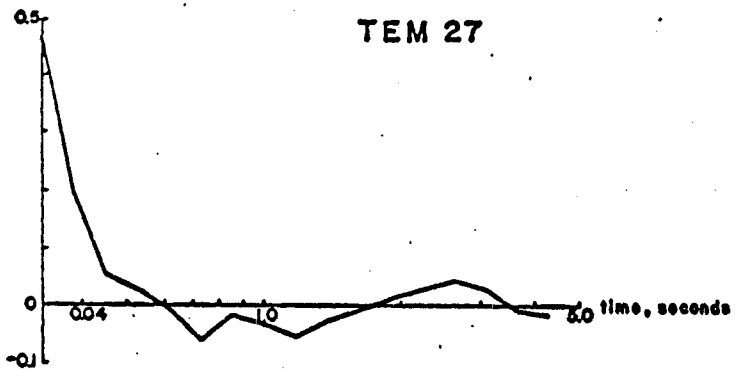
TEM 27
0.5
0
-0.1
0.04
1.0
5.0
time, seconds

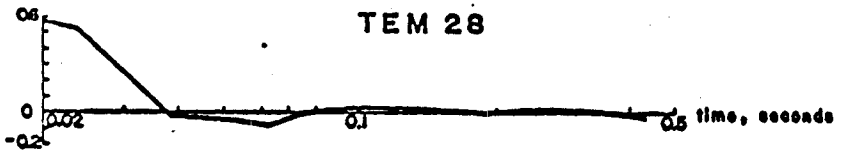
TEM 28
0.6
0
-0.2
0.02
0.1
0.5
time, seconds

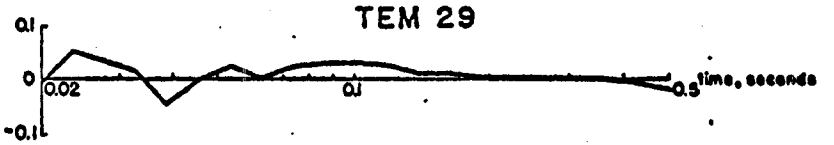
TEM 29
0.1
0
-0.1
0.02
0.1
0.5
time, seconds

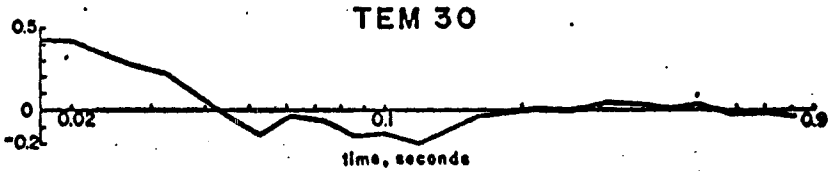
TEM 30
0.5
0
-0.2
0.02
0.1
0.9
time, seconds

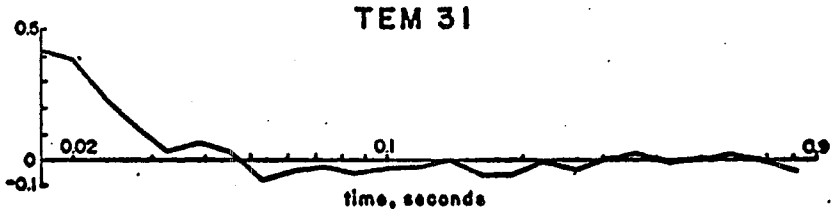
TEM 31
0.5
0
-0.1
0.02
0.1
0.9
time, seconds

Figure B.3. The late-time resistivity function, from equation IV.12 for the transient data plotted in Figure B.1. The numbers at the ends of each trace identify the transient sounding.

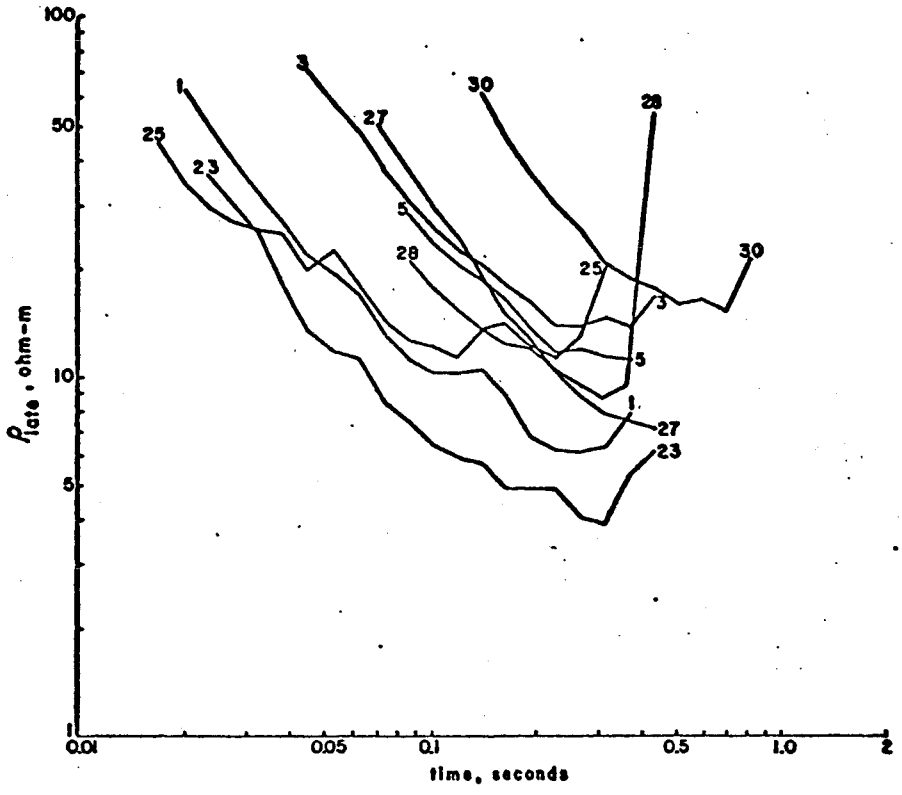
100
50
10
5
1
0.01
0.05
0.1
0.5
1.0
2
time, seconds
ρ_{late}, ohm-m
1
3
27
30
28
25
23
5
28
25
30
3
5
1
27
23

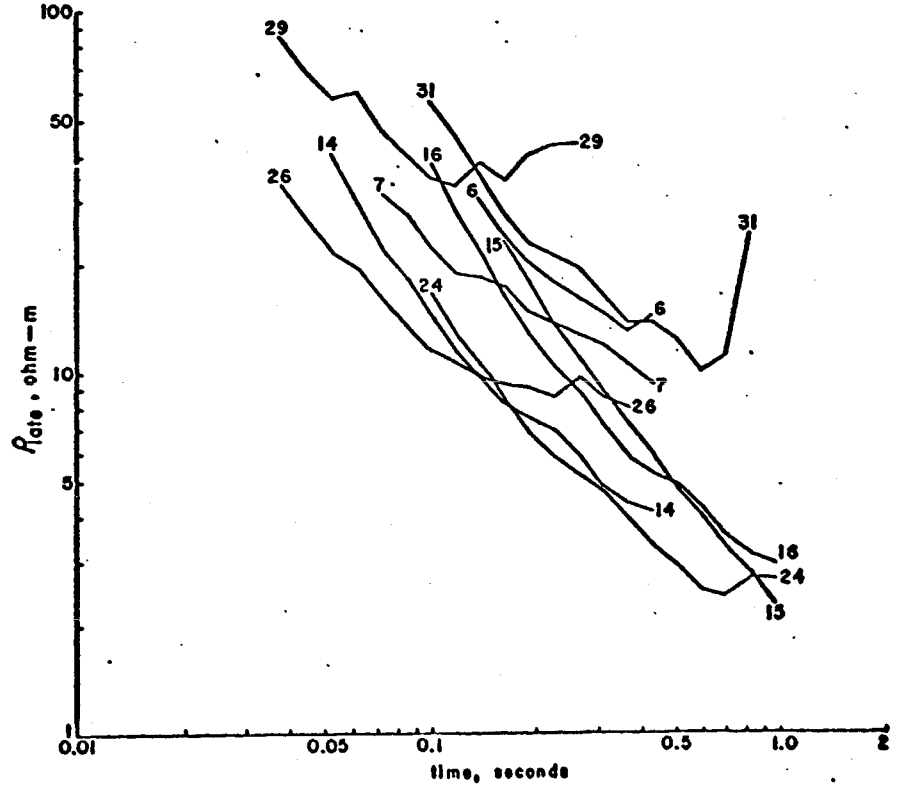
100
50
10
5
1
0.01
0.05
0.1
0.5
1.0
2
time, seconds
ρ_{late}, ohm-m
29
31
14
16
29
26
7
6
31
15
24
6
7
26
14
16
24
15

APPENDIX C: Computer Program Listings

The three programs listed in this appendix have been written in the time-sharing language APL (version APLSV), and were used on an IBM 370/158. They are listed complete with internally required functions.

Davidon's Method

The program DAVIDON simply minimizes a single-valued function using an algorithm described in detail by Fletcher and Powell (1963) and the IBM Scientific Subroutines Package manual. Two FORTRAN versions, called FMFP and DFMFP, are available in this package.

DAVIDON requires a user-supplied program, MODEL, whose output must be the value of the function and its gradient for an input of variables. The example version of MODEL listed here calculates the sum-of-squares function (equation IV.3) and its gradient for an input matrix of data, D, and the three variable vector, $\vec{\theta}$. The user must choose the convergence criterion, PREC (usually 10^{-6}), to start the program and is immediately prompted for an initial guess at the parameters. Each iteration produces a printed line providing the iteration number and the new function value, parameters and gradients. When the convergence criterion is met, the final function value, parameters and gradients are printed, followed by the covariance, correlation and second derivative matrix (equations IV.8 and IV.9). A sample run is shown with all program values explained.

```
      15-6 DAVIDON EX14
INITIAL ESTIMATE:
□:
      0 1 .5
1      .00000000     1.00000000      .50000000 13132.85924002 -7759.63226898 -1400.71225369 -7699.40714797
2     1.42579095     1.25921100     1.91554207  2998.20841371  -648.45995818 -1165.17642719  1199.20325415
3     2.18787031     2.22331353     1.27580678  1834.30677148  2090.75356257   267.01386588  3364.10221184
4     4.65747305      .55621351      .67605581  9940.17248106  5435.84134879   658.08382838     6.92213740
5     1.35409870     3.96696397      .98235931   454.06682967   577.80227625   179.14367611  -822.20111722
6     1.22600300     4.00357077     1.00777113   363.20384069   920.93231430   299.66164485   798.19603443
7      .63597107     4.02021660     1.25122221   158.54706746    98.46062105  -156.99223531   395.11870653
8      .26228198     4.07660477     1.26161211    92.91166251   121.01372856   -66.47398161    85.61269475
9      .11419344     4.73200236     1.29939033    87.16753078   -20.52000264   -17.35468898   -69.28735597
10     .08574848     4.76729771     1.30674896    86.90504597     3.75557519     .07324285    14.95428959
11     .08097148     4.77295676     1.30675952    86.89591043     -.29269294    -.20965242     .07381814
12     .08057135     4.77408417     1.30685571    86.89586879     -.00013961    -.00042204     .00011817
13     .08057036     4.77408557     1.30685582    86.89586879      .00000389     .00000170     .00001393
14     .08057036     4.77408557     1.30685582    86.89586879      .00000389     .00000170     .00001393

VALUE OF FUNCTION MINIMUM 86.8959
GRADIENT 3.894835-6 1.698765-6 1.392925-5
FINAL PARAMETERS 0.0805704 4.77409 1.30686
```

```
      ∇DAVIDON[⎕]∇
    ∇ PREC DAVIDON DATA;KOUNT;N;S;OLD;L;Y;FY;GY;Z;W
[1]   'INITIAL ESTIMATE:'
[2]   F←1↑G←DATA MODEL X←⎕
[3]   G←1↓G
[4]   KOUNT←0×N←⍴X
[5]  DEF:H←(N,N)⍴(N+1)↑1
[6]   →START×⍳KOUNT=0
[7]   F←1↑OLD
[8]   X←(-N)↑OLD
[9]   G←(-N)↑1↓OLD
[10]  →START×(+/|G)>PREC
[11] START:KOUNT←KOUNT+1
[12]  KOUNT; 15 8 ⍕X,F,G
[13]  S←-H+.×G
[14]  OLD←F,G,X
[15]  L←1|¯2×F÷DY←G+.×S
[16]  →DEF×⍳(DY≥0)∨((+/|S)÷+/|G)≤PREC
[17] INT:Y←X+L×S
[18]  FY←1↑GY←DATA MODEL ⍵
[19]  GY←1↓GY
[20]  L←2×L
[21]  →INT×⍳((GY+.×S)<0)∧FY<F
[22]  L←L÷2
[23]  Z←((3×F-FY)÷L)+S+.×G+GY
[24]  W←((Z*2)-(G+.×S)×GY+.×S)*0.5
[25]  L←L×1-((GY+.×S)+W-Z)÷((GY-G)+.×S)+2×W
[26]  Y←X+L←L×S
[27]  F←1↑G←DATA MODEL X
[28]  G←1↓G
[29]  →END×⍳(F<PREC)∨(⌈/|G)<PREC
[30]  →DEF×⍳((|F-1↑OLD)≤PREC*2)∧(⌊/|G)>PREC
[31]  Y←G-(-N)↑1↓OLD
[32]  Z←(L∘.×L)÷L+.×⍉
[33]  H←H+Z-(L∘.×⍉L←H+.×⍉)÷Y+.×H+.×⍉
[34]  →START
[35] END:' '
[36]  'VALUE OF FUNCTION MINIMUM ';1↑OLD
[37]  'GRADIENT ';(⍴X)↑1↓OLD
[38]  'FINAL PARAMETERS ';(1+⍴X)↓OLD
[39]  ' '
[40]  'COVARIANCE MATRIX'
[41]  ' '
[42]  2×H
[43]  ' '
[44]  'CORRELATION MATRIX'
[45]  Z←(⍴H)⍴((¯1+⍳1↑⍴H)⌽2×⍳)[;1]
[46]  (2×H)÷(Z×⍉Z)*0.5
[47]  ' '
[48]  'SECOND DERIVATIVES'
[49]  ⎕H
    ∇
```

```
      RESULT←1 70 FINITE 'BFIELD'
      ⍝RESULT NOW CONTAINS THE RESULTANT RESPONSE FOR
      ⍝    A SEPARATION-SOURCE LENGTH RATIO OF 1 AND AN
      ⍝    AZIMUTH OF 70 DEGREES.

      ⍴RESULT
30
      ⍴TAU
30

      ⍝TAU IS CREATED BY RUNNING FINITE AND CONSISTS
      ⍝    OF THE NORMALIZED TIMES THAT GO WITH RESULT.

      ∇FINITE[⎕]∇
    ∇ Z←R FINITE E;N;T;RX;BX
[1]   R←R[2]
[2]   R←R[1]
[3]   N←⌈5÷((R*2)+0.25-R×0.5×2○RAD R)*0.5
[4]   N←N+2|N
[5]   N←(-÷2×N)+(÷N)×⍳N÷2
[6]   N←(-⌽N),N
[7]   RX←((R*2)+(N*2)+2×R×N×2○RAD R)*0.5
[8]   BX←R×(1○RAD R)÷RX
[9]   TAU←T←0.01××(⍳30)×(⍟10)÷10
[10]  T←T∘.×(R÷RX)*2
[11]  Z←⍕E,' T'
[12]  Z←(÷⍴N)×Z+.×(BX÷1○RAD R)×(R÷RX)*4
    ∇
      ∇RAD[⎕]∇
    ∇ R←RAD D
[1]   R←D×○÷180
[2]   ⍝CONVERTS DEGREES TO RADIANS∇
    ∇
      ∇BFIELD[⎕]∇
    ∇ Z←BFIELD TAU;S
[1]   S←,÷(2×TAU)*0.5
[2]   Z←(⍴TAU)⍴(ERF S)-(2÷(○1)*0.5)×(S+(2÷3)×S*3)××-S*2
    ∇
```

Transient Response of a Finite-Length Horizontal Current Source

The program, FINITE, calculates the response of a finite-length source as if the source were constructed of an even number of separate, smaller sources. This is done by recalculating r and y for each of the source components and then averaging the responses. The example run shown below calculated the vertical magnetic field transient, but the program is sufficiently general to serve for any field component.

```
      ⍝DATA←→MATRIX TO BE PASSED ON TO MODEL.

      ∇MODEL[⎕]∇
    ∇ Z←D MODEL X;Y;R
[1]   Y←X[1]+X[2]×R←X[3] MHOM D[;1]
[2]   Z←(D[;2]-Y)
[3]   Z←Z,[1.5] ¯1
[4]   Z←Z,-R
[5]   Y←X[3]÷2×D[;1]*0.5
[6]   Z←Z,-X[2]×4×(Y*4)×(*-Y*2)÷3×(○D[;1])*0.5
[7]   A←Z[; 2 3 4]
[8]   Z← 1 2 2 2 ×(Z[;1]÷D[;3]*2)+.×Z
    ∇

     ⍝D←→DATA MATRIX
      ⍝X←→PARAMETERS
      ⍝MODEL EVALUATES THE SUM-OF-SQUARES FUNCTION SO
      ⍝THAT
      ⍝          (1↑Z)←→SUM OF SQUARES
      ⍝          (1↓Z)←→(⍴X) PARAMETER GRADIENTS

      ∇MHOM[⎕]∇
    ∇ F←A MHOM T;S
[1]   S←A÷2×T*0.5
[2]   F←(ERF S)-(S+(2÷3)×S*3)×(2÷(○1)*0.5)×*-S*2
    ∇
      ∇ERF[⎕]∇
    ∇ Z←ERF X;A;P;T
[1]   P←0.3275911
[2]   A← 0.254829592 ¯0.284496736 1.421413741 ¯1.453152027
[3]   T←÷1+P×X
[4]   Z←1-(*-X*2)×A+.×⌽T∘.*⍳5
[5]  ⍝ALGORITHM FROM SECTION 7.1.26 IN
[6]  ⍝   ABRAMOWITZ AND STEGUN, HANDBOOK
[7]  ⍝   OF MATHEMATICAL FUNCTIONS.
    ∇
```

REFERENCES

Anderson, W. L., 1973, FORTRAN IV Programs for the determination of the transient tangential electric field about a vertical magnetic dipole for an M-layer earth by numerical integration and digital linear filtering, NTIS report PB-221 240, 24 p.

Bard, Y., 1968, On a numerical instability of Davidon-like methods, Math. of Computation, v. 22, p. 665-666.

Beale, E. M. L., 1960, Confidence regions in non-linear estimation, J. Roy. Statis. Soc., v. B-22, p. 41-76.

Dakhnov, V. N., 1962, Geophysical Well Logging, Colo. Sch. Mines Quart., v. 57, no. 2.

Draper, N. R. and H. Smith, 1966, Applied Regression Analysis, John Wiley and Sons, Inc., New York, 407 p.

Fischer, W. A., D. A. Davis and T. Souza, 1966, Fresh water springs of Hawaii from infrared images, U. S. Geological Survey Hydrologic Atlas, HA-218.

Fiske, R. S. and W. T. Kinoshita, 1969, Inflation of Kilauea prior to its 1967-1968 eruption, Science, v. 165, p. 341-349.

Fletcher, R. and M. J. D. Powell, 1963, A rapidly convergent descent method for minimization, Computer J., v. 6, p. 163-168.

Frischknecht, F. C., 1967, Fields about an oscillating magnetic dipole over a two-layer earth, and application to ground and airborne electromagnetic surveys, Colo. Sch. Mines Quart., v. 62, no. 1.

Glenn, W. E., J. Ryu, S. H. Ward, W. J. Peeples and R. J. Phillips, 1973, The inversion of vertical magnetic dipole sounding data, Geophysics, v. 38, p. 1109-1129.

Grant, F. S. and G. F. West, 1965, Interpretation Theory in Applied Geophysics, McGraw-Hill Book Co., New York, 584 p.

Inman, J. R., 1975, Resistivity inversion with ridge regression, Geophysics, v. 40, p. 798-817.

Jackson, D. B. and G. V. Keller, 1972, An electromagnetic sounding survey of the summit of Kilauea volcano, Hawaii, Jour. Geophys. Res., v. 77, p. 4957-4965.

Jenkins, G. M. and D. G. Watts, 1968, Spectral Analysis and its Applications, Holden-Day, San Francisco, 525 p.

Keller, G. V., 1973, An electrical resistivity survey of the Puna and Kau districts, Hawaii county, Hawaii, unpub. report prepared for the Research Corp. Univ. Hawaii.

_____ and F. C. Frischknecht, 1966, Electrical Methods in Geophysical Prospecting, Pergammon Press, New York, 517 p.

Kraichman, M. B., 1970, Handbook of Electromagnetic Propagation in Conducting Media, U. S. Govt. Printing Office, Washington, D. C., 120 p.

Logan, J., 1961, Estimation of electrical conductivity from chemical analyses of natural waters, Jour. Geophys. Res., v. 66, p.. 2479-2483.

Macdonald, G. A., 1956, The structure of Hawaiian volcanoes, Koninklijk Nederlandsch Geologisch-Mijnbouwkundig Genootschap, Verhandelingen, v. 16, p. 274-295.

_____ and A. T. Abbott, 1970, Volcanoes in the Sea, Univ. of Hawaii Press, Honolulu, 441 p.

Manghnani, M. H., C. S. Rai and T. Hanada, 1976, Physical properties of rocks, in Phase II Progress Report, Hawaii Geothermal Project, p. 50-62.

McMurtry, G. M., P. F. Fan and T. B. Coplen, 1976, Chemical and isotopic investigation of groundwater in potential geothermal areas in Hawaii, Am. J. Sci., in press.

Mundry, E., 1966, The vertical magnetic field of an alternating current dipole for horizontally stratified media, Geophysical Prospecting, v. 14, p. 468-479.

Quist, A. S. and W. L. Marshall, 1968, Electrical conductances of aqueous sodium chloride solutions from 0 to 800° C and pressures to 400 bars, J. Phys. Chem., v. 72, p. 684-703.

Schlichter, L. B. and M. Telkes, 1942, Electrical properties of rocks and minerals, in Handbook of Physical Constants (F. Birch, ed.), Geol. Soc. America Special Paper 36, p. 299-319.

Schwartz, J. H., 1937, Resistivity studies of some salt-water boundaries in the Hawaiian islands, Transactions Am. Geophys. Union, 18th Annual Mtg., part 2, p. 387-393.

Scriba, H., 1974, A numerical method to calculate the electromagnetic field of a horizontal current dipole, Pure Appl. Geophys., v. 112, p. 801-809.

Silva, L. R., 1969, Two-layer master curves for electromagnetic sounding, thesis 1250, Colo. Sch. Mines, 79 p.

Skokan, C. K., 1974, A time-domain electromagnetic survey of the east rift zone, Kilauea volcano, Hawaii, thesis 1700, Colo. Sch. Mines, 150 p.

Stanley, W. D., D. B. Jackson and A. R. Zohdy, 1976, Deep electrical investigations in the Long Valley Geothermal Area, California, Jour. Geophys. Res., v. 81, p. 810-820.

Stearns, H. T., 1965, Geology of the State of Hawaii, Pacific Books, Palo Alto, 266 p.

Vanyan, L. L., 1967, Electromagnetic Depth Soundings (G. V. Keller, trans.), Consultants Bureau, New York, 312 p.

Wait, J. R., 1951, The magnetic dipole over the horizontally stratified earth, Canadian J. Physics, v. 29, p. 577-592.

_____, 1954, Mutual coupling of loops lying on the ground, Geophysics, v. 19, p. 290-296.

_____, 1966, Electromagnetic fields over an anisotropic half-space, Canadian J. Phys., v. 44, p. 2387-2401.

_____ and D. A. Hill, 1973, Excitation of a homogeneous conductive cylinder of finite length by a prescribed axial current distribution, Radio Science, v. 8, p. 1169-1176.

_____ and K. P. Spies, 1969, On the image representation of the quasi-static fields of a line current source above the ground, Canadian J. Phys., v. 47, p. 2731-2733.

Yost, W. J., 1952, The interpretation of electromagnetic reflection data in geophysical exploration-part I, general theory, Geophysics, v. 17, p. 89-105.

Zablocki, C. J., R. I. Tilling, D. W. Peterson, R. I. Christiansen, G. V. Keller and J. C. Murray, 1974, A deep research drill hole at the summit of an active volcano, Kilauea, Hawaii, Geophys. Res. Letters, v. 1, p. 323-326.

Zohdy, A. R. and D. B. Jackson, 1969, Application of deep electrical soundings for groundwater exploration in Hawaii, Geophysics, v. 34, p. 584-600.